The Geometric Stochastic Resonance

and

Rectification of Active Particles

by

Russell Glavey

Doctoral Thesis

Submitted in partial fulfillment of the requirements
for the award of
Doctor of Philosophy of Loughborough University

July 20, 2015

Abstract

This thesis describes the work of three research projects, the background research that motivated the work, and the resultant project findings. The three projects concerned: (i) Geometric stochastic resonance in a double cavity, (ii) Synchronisation of geometric stochastic resonance by a bi-harmonic drive, and (iii) Rectification of Brownian particles with oscillating radii in asymmetric corrugated channels. In the project 'Geometric stochastic resonance in a double cavity', we investigated synchronisation processes for the geometric stochastic resonance of particles diffusing across a porous membrane and subject to a periodic driving force. Non-interacting particle currents were driven through a symmetric membrane pore either parallel or perpendicular to the membrane. Then, harmonic mixing spectral current components were generated by the combined action of parallel and perpendicular drives. The role of the repulsive interaction of particles as a controlling factor with potential applications to the transport of colloids and biological molecules through narrow pores was also investigated.[1]

In 'Synchronisation of geometric stochastic resonance by a bi-harmonic drive', we simulated the stochastic dynamics of an elliptical particle using the Langevin equation. The particle was simultaneously driven by low and high frequency harmonic drives across a porous inter-cavity membrane. It was observed that the particle oscillated out of phase with the low frequency drive. This effect was due to the absolute negative mobility the particle would have exhibited if the low frequency drive had been replaced by a dc static force. It was also observed that the magnitude of this out-of-phase stochastic resonance depends on how the combined action of the driving forces and noise fluctuations affect the particle orientation, and as such was shown to be sensitive to the particle shape. This emphasises the importance of particle geometry, in addition to chamber geometry, to the realisation and optimisation of geometric stochastic resonance.[2]

In the project 'Rectification of Brownian particles with oscillating radii in asymmetric corrugated channels', we simulated the transport of a Brownian

particle with an oscillating radius freely diffusing in an asymmetric corrugated channel over a range of driving forces for a series of temperatures and angular frequencies of radial oscillation. It was observed that there was a strong influence of self-oscillation frequency upon the average particle velocity. This effect can be used to control rectification of biologically active particles as well as for their separation according to their activity, for instance in the separation of living and dead cells.[3]

The background research is described in Chapter One and the research findings are described along with their related projects in Chapters Two and Three.

Acknowledgements

I wish to thank my supervisor Prof: Sergey Savel'ev who epitomises what a Ph.D. supervisor should be. His depth of knowledge, understanding and experience is unfathomable and I am deeply grateful to him that he put it so readily at my disposal. Without him my Ph.D. or this thesis would not have been possible. I wish to thank my co-authors and co-researchers: Prof: Fabio Marchesoni, Dr: Martin P Read, Dr: Pulak K Ghosh and Prof: Franco Nori, with whom I was able to co-publish three research papers. They generously opened up their research group to me and introduced me to the multiplicative power of collaborative research. I wish to thank the staff of the Physics Department of Loughborough University for their warm welcome, continued friendship and professional excellence of teaching, training, researching and administration. I wish to thank my fellow Ph.D. students for their guidance and camaraderie throughout the term of my Ph.D.. I also wish to thank the undergraduate students whom I had the privilege of teaching and learning alongside them. I wish to thank the staff of the Graduate School of Loughborough University for their help, support and guidance throughout the term of my Ph.D.. Their comprehensive list of Professional Development Skills Courses enabled me to develop the ancillary skills necessary to be a confident modern researcher. Moreover, their conference funding enabled me to participate in IEEE-NANO 2012, ICNF2013 and SSPCM2014. I wish to thank the staff of the Disability Office of Loughborough University for their helpful advice, support and the provision of study aids including magnifying glasses and a printer. I also wish to thank them for the provision of a student notetaker. I wish to thank the staff of the Careers and Employability Centre whose helpful advice, guidance and careers fairs enabled me to see and prepare for the onward journey. I wish to thank Loughborough University and the EPSRC for their funding of my Ph.D.. I wish to thank my family and friends for their encouragement and understanding throughout this journey. Finally, I wish to thank everyone at Loughborough University for enabling me to experience a truly universal experience of learning and living in a way no other university can equal.

Contents

1 Stochastic Transport **viii**

1.1 Stochastic Transport in One Dimension 4

1.1.1 Stochastic Transport in One Dimension 5

1.2 Stochastic Transport in Two Dimensions 7

1.2.1 Two Dimensional to One Dimensional - When Effective . 7

1.2.2 Irreducable 2D Problems in Rectification 8

1.3 Stochastic Resonance 11

1.3.1 Stochastic Resonance 11

1.3.2 Entropic Stochastic Resonance 14

1.3.3 Geometric Stochastic Resonance 15

1.4 Rectification 18

1.5 Absolute Negative Mobility 20

1.6 Stochastic Transport: Applications 21

1.6.1 Vortices 22

1.6.2 Colloids 27

1.6.3 Intermission: Bacteria 28

1.6.4 Microswimmers 29

2 Geometric Stochastic Resonance **31**

2.1 Geometric Stochastic Resonance in a Double Cavity 32

2.1.1 Model 33

2.1.2 Synchronisation Mechanisms 36

Longitudinal Drive 36

Transverse Drive 37

2.1.3 Harmonic Mixing 38

2.1.4 Particle Interaction 41

2.2 Synchronisation of Geometric Stochastic Resonance by a bi-Harmonic Drive 44

2.2.1 Model 46

2.2.2 bi-Modal Stochastic Resonance 47

3 Rectification **53**
3.1 Rectification of Brownian Particles 53
3.2 Model 54
3.3 Rectification of Biologically Active Particles 56

4 Conclusions and Outlook **59**

A Programs and Datasets **64**

B Bibliography **65**

List of Figures

1.1 Stochastic transport in a confined geometry model 2
1.2 Mobility in 2D periodic channels 10
1.3 Number of stochastic resonance papers by year 12
1.4 Double well potential $V(x)$ 13
1.5 Entropic stochastic resonance 14
1.6 Chamber shape for geometric stochastic resonance 16
1.7 Geometric stochastic resonance 17
1.8 Vortex ratchet 19
1.9 Absolute negative mobility 21
1.10 Vortex structure and motion 23
1.11 Vortex rectification 24
1.12 Reversible rectification 25
1.13 Time asymmetric rectification 26
1.14 Pili: Extension, adherence and retraction 28

2.1 Geometric stochastic resonance $\bar{x}(D)$ versus noise intensity D . . 34
2.2 Distribution density of residence times versus time periods T_Ω . . 37
2.3 Spectral density of $x(t)$ for two different noise intensities 39
2.4 Geometric stochastic resonance for interacting particles 40
2.5 Resonant behaviour of harmonic mixing components 42
2.6 Amplitude $\bar{x}(D)$ versus magnitude of particle interaction α 43
2.7 Chamber shape for out-of-phase geometric stochastic resonance . 45
2.8 Amplitude of system response $\bar{x}$ versus noise D 48
2.9 Noise dependence of system response parameters. 49
2.10 Dependence of out-of-phase stochastic resonance on the particle elongation ratio b/a 51
2.11 Normalised power spectrum 52

3.1 Brownian particle in a 2D asymmetric corrugated channel 55
3.2 Average velocity versus dc driving force 56

3.3 Average velocity versus oscillating driving force 57

4.1 Citation map 62

Chapter 1

Stochastic Transport

In this first chapter, we introduce stochastic transport in several of its forms including: stochastic resonance, rectification and absolute negative mobility. We define and describe these phenomena, with particular emphasis upon rectification and a form of stochastic resonance called geometric stochastic resonance. We describe some models of stochastic transport and discuss their inherent limitations. We also consider some of the applications of stochastic transport to superconductivity, nanotechnology and biological systems.

The purpose of this introductory chapter therefore is to review the background material necessary to the understanding of the research undertaken and to review the research that motivated that work. Here we wish to set geometric stochastic resonance and rectification in the context of stochastic transport. We wish to justify the use of the overdamped Langevin equation. We also wish to highlight the limitations of modelling stochastic transport in one dimension and the irreducible dynamics of geometric stochastic resonance. Finally we wish to summarise some of the practical applications of the control of stochastic transport.

Throughout this work noise serves as the common characteristic that joins all these apparently disparate topics together. Noise in one form or another is responsible for all the stochastic transport mechanisms we shall have cause to discuss herein: stochastic resonance, geometric stochastic resonance, absolute negative mobility, rectification and more besides. It is the most important prerequisite ingredient for directed transport on the nanoscale and consequently motivates an increasing amount of research as our technologies arrive on the nanoscale and are forced to confront the challenge of achieving directed transport in a noisy environment. Noise and its utility in achieving directed transport on the nanoscale is the common motivator behind the works we present here.

Stochastic transport is defined as the transport of particles by consequence of the constructive interaction of random noise with a system. If the noise was absent the directed transport would cease. Stochastic transport encompasses phenomena such as stochastic resonance, rectification and absolute negative mobility amongst others, all of which we shall define in turn.

To begin our discussion of stochastic transport we will describe a model thereof. The model that we describe here is based upon *Burada et al* and is included for illustrative purposes.[4] Later we will depart from this sample model to more specific models to either illustrate our point or in the case of Chapters Two and Three to describe the models used in our simulations.

Burada et al considered some rigid spherical particles confined in a two or three dimensional channel.[1] For ease of modelling they made some simplifying assumptions. The channel extends along the x axis and has a periodically varying cross-section as shown in Figure 1.1.[4]. The channel has smooth rigid walls and is reflection symmetric about the x axis in two dimensions and axially symmetric about it in three. The channel half-width is described by the well behaved boundary function $W(x)$. The boundaries confine the particles to the channel in such a way that no energy is exchanged in particle-boundary interactions. The possibility of particle adsorption on the boundary walls is also neglected for ease of modelling. *Burada et al* also neglected particle rotations about their centre of mass and the consequent particle-boundary contact forces. The spherical particle's radius is less than the minimum channel half-width such that the particles can move unhindered throughout. This latter consideration is often relaxed in our own models, where particle radius or semi-major axis may exceed the channel half-width at times during the simulation.

In the *Burada et al* model the non-extensive point-like particles are assumed to be in the laminar flow regime whereby they cause little disturbance to the fluid medium through which they pass. Therefore the force on a particle at position $\vec{x} = (x, y, z)$ due to the surrounding fluid medium is given by Stokes' law:

$$\vec{F}_{Stokes} = -\gamma[\dot{\vec{x}} - \vec{v}(\vec{x}, t)], \tag{1.1}$$

where $\vec{v}(\vec{x}, t)$ is the instantaneous fluid velocity in the absence of the particles, $\dot{\vec{x}}$ is the instantaneous velocity of the particles and the friction constant is given by:

$$\gamma = 6\pi\eta R, \tag{1.2}$$

where η is the shear viscosity of the medium and R is the particle radius.[4, 5]

[1] The model presented here and in sections 1.1.1 and 1.2.1 is taken with little alteration from: Burada, P.S. Hänggi, P. Marchesoni, F. Schmid, G. and Talkner, P. (2009), 'Diffusion in Confined Geometries', *ChemPhysChem*, 10, pp. 45 - 54.

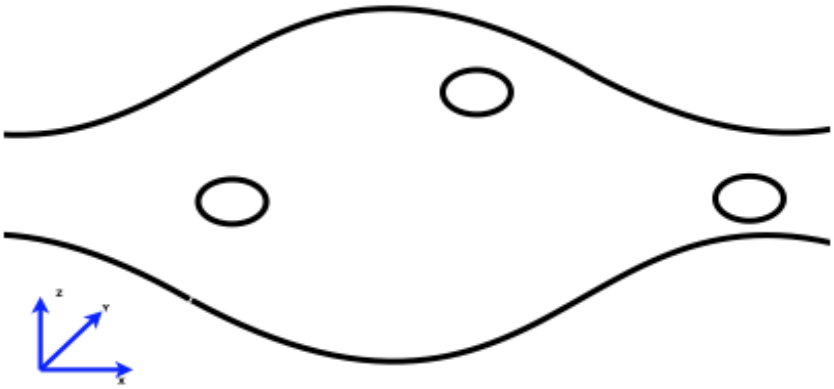

Figure 1.1: Stochastic transport in a confined geometry. Here we present an example model of stochastic transport in a confined geometry. The channel extends along the x axis. It is axially symmetric about the x axis in two and three dimensions. The particles are solid spheres suspended in a fluid medium and no energy is exchanged in particle-boundary interactions.[4].

This is specific to the spherical particles but differs with particle shape.

The fluid medium also exerts a random thermal force F_{th} on the spherical particles. For simplicity of modelling, *Burada et al* assume a homogeneous temperature T throughout the medium and a velocity field that is approximately constant on the scale of the particles R. Therefore to insure thermalization at temperature T, it is only necessary to describe the thermal force as follows:

$$\vec{F}_{th}(t) = \sqrt{2\gamma k_B T}\vec{\xi}(t), \tag{1.3}$$

where k_B is the Boltzmann constant and $\vec{\xi}(t)$ is a standard Gaussian white noise with $\langle\vec{\xi}(t)\rangle = 0$ and $\langle\xi_i(t)\xi_j(t')\rangle = \delta_{ij}\delta(t-t')$ for $i,j = x,y,z$. It is also assumed that other forces acting on the spherical particles can be neglected, such as the force of hydrodynamic interaction between particles and between particles and the boundary. For this latter assumption to hold it is necessary that a low particle number density be considered.[4, 7, 8]

An external force F_{ext} may also act on the particles. For simplicity, *Burada et al* assume that the only external force acting on the particles is a constant external driving force acting along the symmetry axis of the channel, though for stochastic resonance to occur one would require that $F_{ext} = A\cos\omega t$ instead of a constant. The motion of the centre of mass $x(t)$ of a single particle of mass

m is then given by the following equation of motion:

$$m\ddot{\vec{x}} = \vec{F}_{ext} + \vec{F}_{Stokes} + \vec{F}_{th}(t), \tag{1.4}$$

$$m\ddot{\vec{x}} = \vec{F}_{ext} - \gamma[\dot{\vec{x}} - \vec{v}(\vec{x},t)] + \sqrt{2\gamma k_B T}\vec{\xi}(t), \tag{1.5}$$

where $\vec{v}(\vec{x},t)$ is the fluid velocity field which may be time dependent. For particles on the scale of 1μm moving with speeds on the order of 1cms^{-1}, the inertial term $m\ddot{\vec{x}}(t)$ in equations 1.4, 1.5 is negligibly small compared to the other forces acting on the particle.[4] Therefore, provided that the fluid velocity field does not change too rapidly, the particle mass can be set to zero, giving the overdamped limit to the Langevin equation or the so called Smoluchowski approximation. Under these conditions, equation 1.5 simplifies to equation 1.6 after rearrangement.[4, 38]

$$\dot{\vec{x}} = \vec{v}(\vec{x},t) + \frac{1}{\gamma}\vec{F}_{ext} + \sqrt{\frac{2k_BT}{\gamma}}\vec{\xi}(t). \tag{1.6}$$

This Langevin equation is equivalent to a Fokker-Planck equation for the probability density $P(\vec{x},t)$ of a particle to be found at the position x at time t, given by equation 1.7.[4]

$$\frac{\partial P(\vec{x},t)}{\partial t} = -\vec{\nabla}\cdot\vec{J}(\vec{x},t). \tag{1.7}$$

Here $\vec{J}(\vec{x},t)$ is the probability current density given by equation 1.8.[4]

$$\vec{J}(\vec{x},t) = -\left[\vec{v}(\vec{x},t) + \frac{\vec{F}_{ext}}{\gamma}\right]P(\vec{x},t) + \frac{k_BT}{\gamma}\vec{\nabla}P(\vec{x},t). \tag{1.8}$$

In addition to the equation of motion an appropriate set of boundary conditions is also required for a full implementation of a stochastic transport model. These boundary conditions are channel dependent, but in general are made up of two components namely transverse and longitudinal boundary conditions. The longitudinal boundary conditions describe how the particle 'enters' and 'leaves' the channel segment under study, while the transverse boundary conditions describe how the particle interacts with the surrounding walls.

The transverse boundary conditions require that the particle does not penetrate the boundary or adhere to it. This is achieved by implementing a boundary condition such as:

$$\vec{n}(\vec{x})\cdot\vec{J}(\vec{x},t) = 0 \quad \vec{x}\in \text{wall}, \tag{1.9}$$

where $\vec{n}(\vec{x})$ is the unit vector normal to the boundary.[4] Since the particles

are almost point-like solid spheres, this boundary condition is implemented at a radial distance R parallel to the boundary.[4]

The longitudinal boundary conditions in an infinitely long periodic channel such as that depicted in Figure 1.1 are implemented by a boundary rule such as:

$$P(x, y, z, t) = P(x + L, y, z, t), \tag{1.10}$$

where L is the chamber length.[4]

Collectively the equation of motion and the boundary conditions allow the modelling of any stochastic transport through a channel. For this reason we have described the *Burada et al* model. It is from sample models such as this that we depart to specific models in Chapters Two and Three.

1.1 Stochastic Transport in One Dimension

We now consider stochastic transport in one dimension: its success and failures.

At first it may seem that stochastic transport was modelled in one dimension for reasons of simplification of simulation, whilst this may have been a consideration it was not the motivating factor. Stochastic transport came to be modelled in one dimension because it was realised that Brownian motors achieved directed transport on the nanoscale by means of confining particles to constrained geometries of effectively one dimension wherein their Brownian motion was used to assist directed transport. Therefore, the study of stochastic transport in confined geometries sought to reproduce the physical reality by using one-dimensional models. It should be added that Brownian motion is the continual random motion of small particles suspended in a liquid or gas by consequence of their being bombarded by still smaller particles of the medium namely atoms or molecules. Furthermore, Brownian motors are microscale to nanoscale devices that use thermal noise to assist directed motion by overcoming intervening energy barriers.[26]

Here therefore, we will begin with a description of a one dimensional model of stochastic transport developed from its two and three dimensional counterparts. We will then consider its successes and failures. The latter have led to the need for the description of some stochastic transport phenomena, for example, geometric stochastic resonance, in higher dimensions rather than the customary one dimensional models described here.

1.1.1 Stochastic Transport in One Dimension

To model the stochastic transport of spherical particles in a two or three dimensional periodically constrained geometry in one dimension, we begin with an ideal case, namely the stochastic transport of a single point-like particle on a one dimensional energetic potential $V(x)$ with period L, such that, $V(x) = V(x+L)$. The potential $V(x)$ may also be reflection symmetric, such that $V(x) = V(-x)$, if we happen to be considering a ratchet potential. The particle's stochastic dynamics can then be modelled by the Langevin equation:

$$m\ddot{x} = -V'(x) - \gamma\dot{x} + F + \sqrt{2\gamma k_B T}\xi(t), \tag{1.11}$$

where m is the particle mass, x is the particle position, γ is the coefficient of friction, F is an external driving force, k_B is the Boltzmann constant, T is the temperature and $\xi(t)$ is a Gaussian white noise. This is consistent with equation 1.5, if we let $F_{ext} = -V'(x) + F$ and $v(x,t) \equiv 0$.[4, 6]

As mentioned previously, for systems on the scale of 1μm or less, particle dynamics can be described to a good approximation by the overdamped limit to equation 1.11, wherein the inertia term $m\ddot{x}$ can be dropped owing to its negligible contribution to particle dynamics. This leads to the Smoluchowski approximation to the Langevin equation.[4]

$$\gamma\dot{x} = -V'(x) + F + \sqrt{2\gamma k_B T}\xi(t). \tag{1.12}$$

The overdamped particle remains trapped at a minimum of the tilted energetic potential as long as the driving force F is less than the depinning threshold F_p, $(F \leq F_p)$, where $F_p = max(V'(x))$. Drift results only from noise-induced hopping between adjacent minima. When the driving force F exceeds F_p, $(F > F_p)$, there are no such minima and the particle moves in the direction of the driving force with an average speed approaching F/γ.[4] This behaviour is described by the mobility formula:[4]

$$\mu(F) \equiv \frac{\langle\dot{x}\rangle}{F}, \tag{1.13}$$

where $\langle\dot{x}\rangle$ is given by:

$$\langle\dot{x}\rangle \equiv \frac{\langle x(t)\rangle}{t}. \tag{1.14}$$

As the particle moves due to the driving force F, the random hops cause a spatial dispersion of the particle about its average position $\langle x(t)\rangle$.[4] This is

described by the normal diffusion coefficient:[4]

$$D(F) \equiv \lim_{t\to\infty} \frac{\langle x(t)^2\rangle - \langle x(t)\rangle^2}{2t}. \tag{1.15}$$

These formulas for the nonlinear mobility 1.13 and the normal diffusion coefficient 1.15 can be reformulated to describe stochastic dynamics on a 1D substrate.[4] However, as we shall see in subsection 1.2.1, they fail to reproduce the experimental results for large driving forces or sharp confining geometries, thus limiting the applicability of the 1D reductionist approach.

For the spherical particles that we are considering moving in the static fluid medium of a two or three dimensional confining geometry, as the particle radius approaches zero, elastic contact particle-particle interaction forces can be neglected. Moreover, the particle interactions with the boundary walls can be modelled by equation 1.9, as long as particle-boundary interactions caused by the fluid medium can also be neglected.[4, 7, 8]

If we assume that these particles are suspended in a static medium and are subjected to an external driving force $F(x,t)$ along the channel axis, then their overdamped Brownian dynamics can be modelled by either the Langevin equation 1.6, 1.12 above, or by the corresponding Fokker-Planck equation 1.7, both with $\vec{v}(\vec{x},t) \equiv 0$. Unfortunately for the generic periodic channel $W(x)$, represented in Figure 1.1, no exact analytical solution to the Fokker-Planck equation with the boundary conditions of equation 1.9 is known. Consequently an approximate solution has to be found by reducing the problem to that of driven Brownian motion on an effectively one dimensional periodic potential. In the process of reduction, the confining geometries of the two or three dimensional model are replaced by the entropic barriers of the one dimensional model.[4]

When $F = 0$, the Brownian dynamics of these particles in two or three dimensions is approximated by a Fick-Jacobs kinetic equation in the one dimensional model with a spatially dependent diffusion coefficient:

$$\frac{\partial P(x,t)}{\partial t} = \frac{\partial}{\partial x}\left[D(x)\sigma(x)\frac{\partial}{\partial x}\frac{P}{\sigma(x)}\right], \tag{1.16}$$

where $\sigma(x)$ is a dimensionless channel cross-section parameter best fitted by $\sigma(x) = 2W(x)/L$ in two dimensions and $\sigma(x) = \pi W^2(x)/L^2$ in three dimensions. [4, 11, 79, 80] The x-dependent diffusion coefficient improves the accuracy of the Fick-Jacobs kinetic equation and extends its validity to larger amplitudes of $W(x)$:

$$D(x) = \frac{D_0}{[1 + W'(x)^2]^\alpha}, \tag{1.17}$$

where values of $\alpha = 1/3$ in two dimensions and $\alpha = 1/2$ in three dimensions, give

the best results for wall curvature effects in the one dimensional model.[4, 12, 80] However, as already mentioned, the x-dependent diffusion coefficient retains its attendant problems of accuracy at larger values of amplitude and driving force, as shall be seen in section 1.2.1.

For a weak driving force F along the channel axis, the Fick-Jacobs kinetic equation can be expressed as:

$$\frac{\partial P}{\partial t} = \frac{\partial}{\partial x} D(x) \left[\frac{\partial P}{\partial x} + \frac{A'(x)}{k_B T} P \right], \tag{1.18}$$

where $A(x) = E(x) - TS(x)$ is the free energy made up of an energy term $E(x) = -Fx$, and an entropic term, $S(x) = k_B \ln \sigma(x)$ [4, 13, 80] For a periodic confining geometry, $A(x)$ takes the form of a periodic tilted energetic potential. For a straight channel, $W(x) = 0$, the entropic term vanishes and the particle is subject only to the external driving force. When $F = 0$ the free energy is purely entropic and equation 1.18 reduces to the Fick-Jacobs kinetic equation 1.16.[4]

1.2 Stochastic Transport in Two Dimensions

1.2.1 Two Dimensional to One Dimensional - When Effective

Two key parameters that measure the stochastic dynamics of the reduced 2D to 1D model described by the Fick-Jacobs equation 1.18 are the nonlinear mobility 1.13 and the effective diffusion coefficient 1.15.[2][4, 15, 16, 17] In the model, the variable f is a dimensionless force defined as the ratio between the work done by the force F on the particle to drag it a distance L and the thermal energy $k_B T$, $f = FL/k_B T$.[4] An important difference between a strictly energetic 1D model and one containing an entropic component, such as the one considered here in Figure 1.1, is that for a particle moving in a one dimensional periodic potential $V(x)$, the barrier $\triangle V$ separating the potential minima provides an additional energy scale to that of FL and $k_B T$. Consequently, the particle's dynamics is determined by two dimensionless energy parameters: $\triangle V/k_B T$ and $FL/k_B T$. However, Brownian transport in a two or three dimensional periodically corrugated channel is controlled only by the dimensionless force f.[4, 13]

To test the agreement of the one dimensional model with its two and three

[2] As stated previously, the model presented here and in section 1.1.1 is reproduced with little alteration from: Burada, P.S. Hänggi, P. Marchesoni, F. Schmid, G. and Talkner, P. (2009), 'Diffusion in Confined Geometries', *ChemPhysChem*, 10, pp. 45 - 54.

dimensional counterparts, the f-dependence of the nonlinear mobility and the effective diffusion coefficient were compared with the results from numerical integration of the two dimensional Langevin equation 1.6.[4, 12] The particles were confined in a geometry whose channel walls were described by the sinusoidal boundary function $W(x)$.[4]

It was found that in contrast to a purely energetic one dimensional model, the nonlinear mobility decreases for increasing magnitude of the thermal noise. Moreover, the effective diffusion coefficient increases, with maximum exceeding the free diffusion constant D_0.[4, 12, 18]

For low values of the control parameter f, it was found that the predicted values of the nonlinear mobility and the effective diffusion coefficient matched the predictions of the two dimensional Langevin equation. However at higher values of the control parameter f deviations arise. Most importantly, the curves for the effective diffusion coefficient and the nonlinear mobility fail to reach the correct asymptotic limit, (1 as $f \to \infty$). The reason for this is that the assumption of a transversally uniform density distribution, introduced in the formulation of the Fick-Jacobs 1D model to eliminate transverse coordinates is no longer valid in the presence of a strong driving force.[4] The agreement between the 1D model and the 2D alternative improve for smooth modulations of the boundary wall, that is, for small boundary slopes $|W'(x)|$.[4, 12, 18]

A method of assessing the validity of the stationary state solutions of the Fick-Jacobs model 1.18 can be formulated by comparing the characteristic time scales associated with the model, namely the diffusion time in the transverse direction, the longitudinal direction and the drift time required for the driving force F to drag the particle one channel length.[4] The assumption of a uniform probability distribution in the transverse direction required by the Fick-Jacobs model is valid only if the transverse diffusion is sufficiently fast relative to both the diffusive and the drift longitudinal motions.[4, 18] The value of the critical force parameter f_c above which the Fick-Jacobs model fails, depends upon the remaining free parameters of the specific model.[4]

Thus the Fick-Jacobs model fails to agree with the two-dimensional Langevin model for large modulations of the boundary wall or large driving forces. In this regime a different method of modelling to that of the one dimensional reductionist approach is required.

1.2.2 Irreducable 2D Problems in Rectification

The inadequacy of the Fick-Jacobs model to correctly approximate stochastic dynamics as described in Section 1.2.1 is further illustrated by the case of two-dimensional rectification effects in artificial channels. Both the particle current

pumped by a transverse ac bias and the gating mechanism caused by a transverse ac bias on a driven longitudinal particle current cannot be explained by the Fick-Jacobs approach, and this is described by *Marchesoni et al.*[3][19]

In this example, the stochastic dynamics was modelled in the two dimensional channel shown inset in Figure 1.2. The channel had periodic boundaries such that $W(x + x_L) = W(x)$. The Fick-Jacobs model was based upon the assumption of a uniform probability density in the y direction. This necessitated narrow channel boundaries $W(x) \ll x_L$ and small amplitude boundary modulations $|W'(x)| \ll 1$. If these assumptions were satisfied, the reduced probability density $P(x, t)$ was described by the following Fick-Jacobs equation.[19, 79]

$$\frac{\partial}{\partial t}P(x,t) = \frac{\partial}{\partial x}D(x)\left[\frac{\partial}{\partial x} + \frac{V_L'(x)}{kT}.\right]P(x,t). \tag{1.19}$$

Note: this is the same as equation 1.18. The effective potential $V_L(x)$ was described by equation 1.20, where it was assumed that $|W'(x)| \ll kT/Fx_L$ and $|W'(x)| \ll kT/Gy_L$.[19, 21]

$$V_L(x) = -Fx - kT\ln\left[2\frac{kT}{G}\sinh\frac{GW(x)}{kT}\right]. \tag{1.20}$$

Here F was a longitudinal driving force and G was a transverse driving force.[19, 20]

In the alternative approach, the stochastic dynamics of the overdamped Brownian particle were modelled in the two dimensional channel by the 2D Langevin equation 1.21.[19]

$$\frac{d\vec{r}}{dt} = -F\vec{e}_x - G\vec{e}_y + \sqrt{kT}\vec{\xi}(t). \tag{1.21}$$

As before, $\vec{e}_x$,$\vec{e}_y$ were the unit vectors along the x and y axes respectively and $\vec{\xi}(t) = [\xi_x(t), \xi_y(t)]$ was a zero mean Gaussian white noise with autocorrelation function given by equation 1.22.[19]

$$\langle \xi_i(t), \xi_j(t')\rangle = 2\delta_{i,j}\delta(t - t'). \tag{1.22}$$

Here $i, j = x, y$. The longitudinal driving force F was kept constant and the transverse driving force G had a sinusoidal modulation $G(t) = G\cos(\Omega t)$. The boundaries were perfectly reflecting and the channel bottlenecks were kept to $\Delta \ll y_L$. The channel asymmetry was controlled by the variation of the parameter $x_0/x_L \in [0, 0.5]$. With the introduction of dimensionless units $x \to x/x_L$,

[3]The results described here are from: Marchesoni, F. and Savel'ev, S. (2009), 'Rectification currents in two-dimensional artificial channels', *Physical Review E*, 80, 011120.

$y \to y/y_L$ and $t \to (kT/x_L y_L)t$, it could be shown that for any given geometry, the stochastic dynamics described by equation 1.21 could be controlled by the rescaled forces $Fx_L/kT, Gy_L/kT$ and possibly $x_L y_L \Omega/kT$. The chamber geometry was such that $y_L/x_L = 1$, thus neither Fick-Jacobs condition was satisfied.[19]

In this environment it was found that in the presence of a longitudinal dc driving force F and in the absence of a transverse driving force G, the particle underwent behaviour that could not be explained by the Fick-Jacobs approach. In particular, as shown in Figure 1.2, the graphs for $\mu(F)$ against F/kT were determined by the channel geometry. Furthermore, the mobilities $\mu_\pm(0)$ were weakly dependent upon x_0 contrary to the predictions of the Fick-Jacobs model in equation 1.19.[19, 22] This result also emphasised the impact of chamber geometry upon stochastic transport and informed our own work.

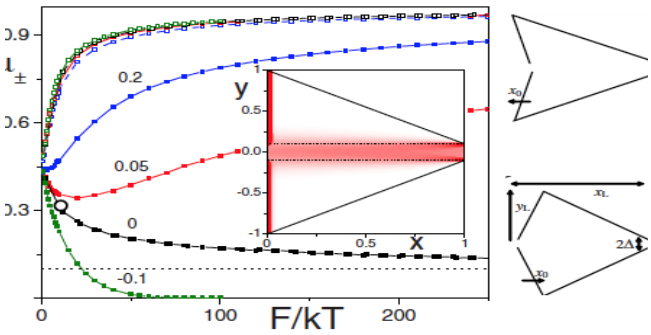

Figure 1.2: Mobilities $\mu_\pm$ versus F/kT for the periodic channel shown inset with $G = 0, T = 0.1$ and various x_0 (given). The mobilities μ_+ are represented by open symbols and μ_- by solid symbols. The asymptote $\mu_-(\infty) = 0.1$ is represented by the dotted line. The inset shows a particle beam corresponding to the μ_- mobility encircled in the main panel with $x_0 = 0$.[19] For further details see reference [19].

In the case of a transverse ac driving force $G(t)$ with frequency $\nu_\Omega = \Omega/2\pi$ and in the absence of a longitudinal driving force ($F = 0$), the Fick-Jacobs model predicted a ratchet potential $V_L(x)$ given by equation 1.20, subject to a time pulsation with frequency $2\nu_\Omega$. According to the Fick-Jacobs model rectification

would then occur in the hard direction ($\mu_-(F)$) and disappear for $G \to \infty$.[19, 95] However, the 2D Langevin equation 1.21 showed that in the case of the most asymmetric channel geometry ($x_0 = 0$), the graphs for the net current v versus G were negative for all pulsation frequencies. This behaviour was the result of an interplay between the transverse and longitudinal diffusions.[19] The disagreement with the Fick-Jacobs predictions was due to their assumption of uniform diffusion in the transverse direction.[19]

Finally, in the case of a combination of a dc driving force F and a transverse periodic driving force $G(t)$ in a channel with $x_0 = 0$, it was found that the Fick-Jacobs model proved inadequate once more. According to the Fick-Jacobs formalism of equations 1.19 and 1.20, optimal gating would have occurred when the particle crossed the unit cell with ballistic time approximately equal to an integer number of half G periods. However results from the 2D Langevin model showed that the peaks corresponding to odd integer values were strongly suppressed.[19] The reason for this suppression could only be understood in terms of the 2D Langevin model and was due to the fact that an unbiased particle beam entering the unit cell from the right was split into two parallel beams. The periodic drive $G(t)$ deviated the two beams across the channel axis to opposite sides of the chamber. They met again in the centre of the channel every full $G(t)$ cycle. Consequently, they met in the centre of the channel at the left bottleneck for n even and were more likely to hit the walls for n odd, with follow on consequences for their respective mobilities. This could not be discerned from the Fick-Jacobs formalism wherein a uniform transverse diffusion was assumed.[19]

These deficiencies in the analysis of stochastic dynamics and boundary effects in a 2D channel as modelled by the Fick-Jacobs formalism highlight once more the short comings of the method and the benefits of adopting a 2D Langevin approach such as we have in our models presented in Chapters Two and Three.

1.3 Stochastic Resonance

1.3.1 Stochastic Resonance

Stochastic resonance is the phenomenon whereby noise, formerly thought to be a hindrance to signal uptake, can actually help a nonlinear system by enhancing its sensitivity to a weak external signal or driving force, and amplify and optimise that signal. It requires three prerequisites: (i) an energy activation barrier or threshold, (ii) a weak coherent input, such as a periodic signal or driving force and (iii) a source of noise that is either part of the system or that adds to the input signal. With these three requirements met, the system

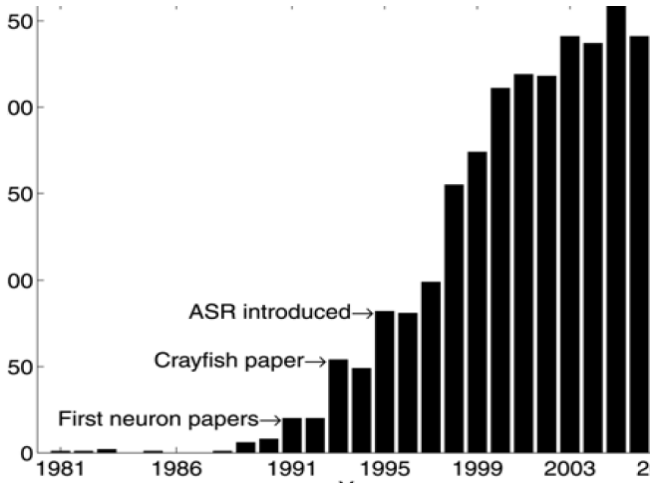

Figure 1.3: Frequency of stochastic resonance papers by year between 1981 and 2007. The labels indicate some significant milestones in stochastic resonance research. Here ASR denotes aperiodic stochastic resonance, see reference [77].[14]

manifests a resonant-like behaviour that is a function of the noise intensity. This behaviour gives rise to its name stochastic resonance.[77]

The generic nature of this definition attests to the pervasive nature of the phenomenon. Stochastic resonance has been demonstrated in fields as diverse from one another as the earth's glaciation cycle, (where it was first demonstrated), and neurosensory systems in biophysics, as bistable chemical reactions and the dynamics of vortices in type II superconductors. An adequate description of the range of stochastic resonance phenomena is beyond the scope of this work. For more the reader is referred to two review papers a decade apart which treat of its growing importance and diversity, [77] and [26]. Here we can only hint at its pervasive nature using Figure 1.3.[77]

To further illustrate our definition of stochastic resonance, we consider the following sample model.[4] The stochastic dynamics of an overdamped Brownian particle in a bistable potential and in the presence of noise and a periodic driving force can be modelled by the following Langevin equation.[77]

$$\dot{x}(t) = -V'(x) + A_0 \cos(\Omega t + \phi) + \xi(t). \tag{1.23}$$

Here $V(x)$ is the bistable potential, see Figure 1.4. It is reflection symmetric

[4]The model described here is from Gammaitoni, L. Hänggi, P. Jung, P. and Marchesoni, F. (1998), 'Stochastic Resonance', *Reviews of Modern Physics*, 70, pp. 223 - 287.

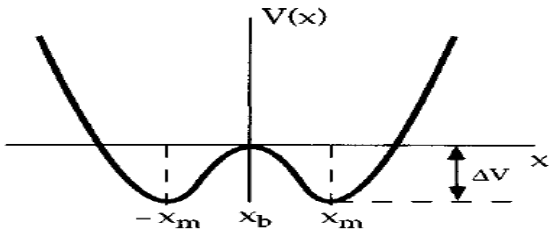

Figure 1.4: A bistable potential $V(x)$ with minima at $\pm x_m$ and intervening threshold ΔV. In the presence of a sub-threshold periodic driving force and noise a Brownian particle confined in this system can undergo stochastic resonance.[77]

and represented by the following quartic equation.

$$V(x) = -\frac{a}{2}x^2 + \frac{b}{4}x^4. \tag{1.24}$$

This can be re-expressed as a dimensionless equation by means of an appropriate scale transformation.

$$V(x) = -\frac{1}{2}x^2 + \frac{1}{4}x^4 \tag{1.25}$$

The zero mean Gaussian white noise $\xi(t)$ in equation 1.23 is given by the auto-correlation function:

$$\langle \xi(t)\xi(0) \rangle = 2D\delta(t). \tag{1.26}$$

Here and in equation 1.23 D is the noise intensity. The potential $V(x)$ is bistable with minima located at $\pm x_m$, with $x_m = 1$. The height of the potential barrier between the minima is given by $\Delta V = \frac{1}{4}$.[77] As we shall see later this potential can be energetic, entropic, a mixture of both, or replaced by a constrained geometry.[77]

It should be added that in the aftermath of the original papers on stochastic resonance by *Benzi et al* a slow but inevitable paradigm shift in the way we think about noise occurred: no longer did we exclusively seek to exclude noise from our systems but began to consider instead how it might be constructively used within them.[131] This shift in thinking was timely as more of our technological systems began to arrive at the nanoscale where noise is inescapable.

1.3.2 Entropic Stochastic Resonance

Entropic stochastic resonance is a form of stochastic resonance that may occur when a Brownian particle is confined in a constrained geometry. The uneven boundaries lend an entropic contribution to the normally energetic potential $V(x)$. In the presence of a periodic driving force, the Brownian particle may undergo a resonant behaviour that can be optimised by an appropriate noise intensity. This form of stochastic resonance may be at work in soft condensed matter and biological systems where Brownian particles move through cavities, pores and other narrow channels whose size and shape can affect the stochastic resonance mechanism. Entropic stochastic resonance may assist the transport of molecules across cell membranes. Consequently, this phenomenon is of interest to nanotechnologists who can potentially use it to assist in the transport of nanodevices.[20, 110, 111]

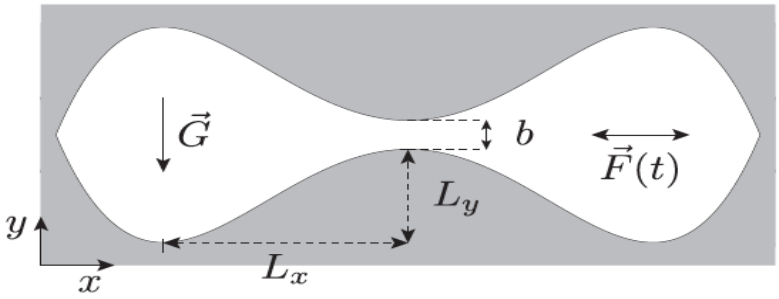

Figure 1.5: A confining geometry with smooth boundaries in which a particle may experience entropic stochastic resonance. The Brownian particle is driven by a sinusoidal driving force $\vec{F}(t)$ along the x axis for some cases and a constant transverse driving force $\vec{G}$ is applied along the y axis. L_x, L_y and b are geometrical parameters of the boundary function W.[20]

To distinguish it from energetic stochastic resonance, we briefly consider the 2D Langevin model of entropic stochastic resonance. For a Brownian particle confined in a constrained geometry, as shown in Figure 1.5 and subject to a sinusoidal force $F(t)$ along the x axis and a constant force G along the y axis,

the resultant 2D dynamics can be described by the following Langevin equation in the overdamped limit:

$$\gamma\frac{d\vec{r}}{dt} = -G\vec{e}_y - F(t)\vec{e}_x + \sqrt{\gamma k_B T}\vec{\xi}(t).[20] \tag{1.27}$$

Here, $\vec{r}$ is the position vector of the particle, γ is the friction coefficient, $\vec{e_x}$, $\vec{e_y}$ are the unit vectors along the x and y directions respectively and $\vec{\xi}(t)$ is the Gaussian white noise with auto-correlation function $\langle\xi_i(t)\xi_j(t')\rangle = 2\delta_{ij}\delta(t-t')$ for $i,j = x,y$. Equation 1.27 can be re-expressed in the dimensionless form below.

$$\frac{d\vec{r}}{dt} = -G\vec{e}_y - F(t)\vec{e}_x + \sqrt{D}\xi(t).[20] \tag{1.28}$$

In this equation, the bistable potential energy term is absent unlike in equation 1.23. This is because the Brownian dynamics is instead constrained by the entropic restrictions associated with the confining geometry. There is good agreement between this 2D Langevin model and a 1D reductionist approach for smooth modulations of the potential function, that is $|W'| \ll 1$, where W is the function describing the channel boundaries.[20]

1.3.3 Geometric Stochastic Resonance

Geometric stochastic resonance is a from of stochastic resonance that can occur when a Brownian particle is moving between two cavities connected by a porous membrane, such as in Figure 1.6, when subjected to a periodic driving force and causes it to exhibit a resonant behaviour with properties that strongly depend upon the confining geometry. This form of stochastic resonance does not require an energetic or an entropic barrier to occur but can be considered as a purely geometric effect. The magnitude of this form of stochastic resonance is sensitive to the geometry of the cavities and the pores through which it passes and has its own optimal synchronisation conditions. This form of stochastic resonance was explored by *Ghosh et al* and is described below.[66]

In this model the overdamped dynamics of a Brownian particle freely diffusing in a two dimensional suspension fluid contained in the two symmetric cavities shown in Figure 1.6 and connected by a narrow pore in the partition membrane was modelled by the following 2D Langevin equation:

$$\frac{d\vec{r}}{dt} = -A(t)\vec{e}_x + \sqrt{D}\vec{\xi}(t). \tag{1.29}$$

As before, $\vec{e}_x, \vec{e}_y$ were the unit vectors along the x and y axes respectively, $\vec{\xi}(t) = (\xi_x(t), \xi_y(t))$, were zero mean Gaussian white noises with autocorrelation functions $\langle\xi_i(t)\xi_j(t')\rangle = 2\delta_{ij}\delta(t-t')$ with $i,j = x,y$. The ac drive was given

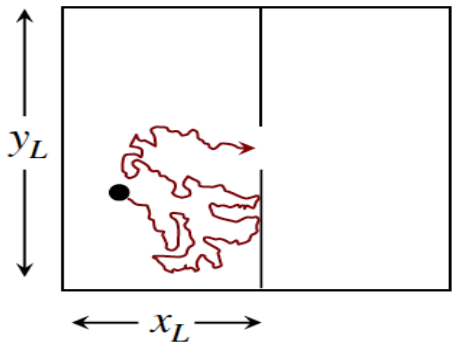

Figure 1.6: A Brownian particle freely diffusing in a suspension fluid contained in the two dimensional symmetric cavities. The cavities were separated by a partition membrane perforated by a pore. The dimensions of the cavity were such that $x_L = y_L = 1$ and $\Delta = 0.1$ was the pore width. However, the values of x_L and Δ could be varied.[66]

by $A(t) = A_0 \cos(\Omega t)$ consequently the resultant Brownian trajectories had a harmonic component $\bar{x}(D)\cos[\Omega t - \phi(D)]$ whose amplitude $\bar{x}$ is plotted against D in Figure 1.7.[66, 1]

Different pore geometries were tested for their affect upon stochastic resonance including a funnel, spout and a simple perforation, see [66]. In the presence of the latter this form of stochastic resonance showed some distinctive characteristics. Firstly, the amplitude of the Brownian particle $\bar{x}(D)$ peaked for a noise intensity D_{max}, where D_{max} itself was an increasing function of Ω. Secondly, stochastic resonance was restricted to $A_0 > A_c$ and $\Omega < \Omega_c$. This is different from ordinary stochastic resonance where no critical value of the drive parameters is required. Thirdly, in the graphs of $\bar{x}(D)$ versus D, $\bar{x}(D)$ decayed in accordance with D^{-1}. This is faster than in any 1D bistable potential and indicates the irreducible nature of geometric stochastic resonance and the need for a discrete 2D model.[66, 1]

As can be seen in Figure 1.7, optimal stochastic resonance is sensitive to both the geometry of the cavities and the pore width. Consequently, geometric stochastic resonance can be affected and controlled by cavity and pore geom-

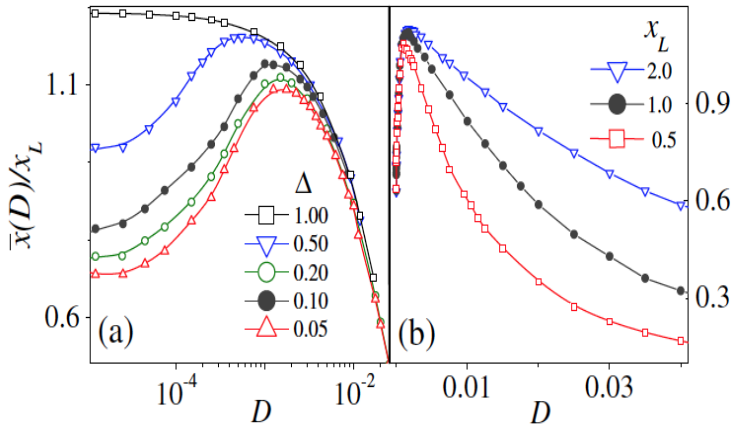

Figure 1.7: The classic graph demonstrating stochastic resonance, $\bar{x}(D)$ versus D. Graph (a) shows how optimal stochastic resonance is affected by the pore width Δ, values inset. Graph (b) shows how optimal stochastic resonance Is affected by the chamber width x_L. The other parameters used were $y_L = 1$, $A_0 = 0.045$, $\Omega = 0.005$ and in (a) $x_L = 1$ and in (b) $\Delta = 0.1$.[66]

etry, this motivated our investigation of particle geometry and the variation thereof. The peaks of the $\bar{x}(D)$ versus D graph occur for certain values of the noise strength D_{max} which weakly depend upon A_0 and increase with Ω. Geometric stochastic resonance is different from ordinary stochastic resonance in that particle transitions between the stable states of the cavities do not depend upon an activation rate or an intervening energy barrier. This form of stochastic resonance is due to the effect of the 2D geometry upon the stochastic dynamics and is irreducible to a 1D model with an entropic potential. Consequently, the 1D Fick-Jacobs approximation is inapplicable here.[66, 1]

Geometric stochastic resonance has practical applications in the control of vortex dynamics in type II superconductor devices. These devices include flux qubits in a potential quantum computers, superconducting quantum interference devices (SQUIDs) and superconducting rf filters. Ion beam lithography can be used to construct sharp confining geometries such as required for geometric stochastic resonance on the surface of type II superconductors. Consequently, vortices can be trapped in vortex boxes connected by a membrane pore with binding energies on the order of $\Phi_0^2 L_t/\lambda^2$, where Φ_0 is the magnetic flux quan-

tum, λ is the London penetration depth and L_t is the vortex trap depth. The density of vortices $n = H/\Phi_0$ can be controlled by the magnetic field intensity H. At low vortex densities, $H \leq \Phi/\lambda^2$, the vortex dynamics is not dictated by vortex-vortex interactions. In this regime AC drives and noise sources generated from independent currents can be used to manipulate vortices through Lorentz forces and control their dynamics in the confined geometries of these superconducting devices. Geometric stochastic resonance offers a very practical way of controlling vortex dynamics in the vicinity of delicate operations on type II superconducting devices.[66, 112, 113]

1.4 Rectification

Rectification is the process of turning the unbiased fluctuations in a system into the directed transport of particles. One way in which this is accomplished is by the use of ratchets. These are devices that are capable of transporting particles in a periodic structure with non-zero macroscopic velocity, although on average no macroscopic force is acting. This is achieved through the breaking of temporal and/or spatial symmetry.[94, 95, 96, 97] Here we consider vortex rectification using spatial asymmetry, as an example. Later in Section 1.6.1, we consider vortex rectification by means of temporal asymmetry.

One obstacle retarding the application of type II superconductor devices is the presence of trapped vortices within the superconductor. These can penetrate the superconductor from sources as weak as the Earth's magnetic field. Once present they cause the dissipation of energy from the superconductor by causing electrical resistance and generation of thermal noise. This in turn limits the lower sensitivity of these devices such as is the case with SQUID magnetometers. Consequently, much effort has been expended in either pinning the vortices in place or flushing them out. Ratchets offer the possibility of achieving the latter through vortex rectification. Here we briefly consider an example of vortex rectification achieved through the breaking of spatial asymmetry in two back to back ratchets.[53, 114]

However, while ratchets have achieved rectification through the breaking of time and or spatial asymmetry, the focus has been on the ratchet structure or drive, little attention has been focused on the particle itself: its geometry and variation in time. Yet vortices are not point like particles, but extensive, and their size can be varied by variation of the magnetic field intensity or temperature. Consequently, their impact upon rectification must also be considered as they offer an additional means of external control and optimisation of the process.

For a thin film of a type II superconductor in a magnetic field H, as shown in

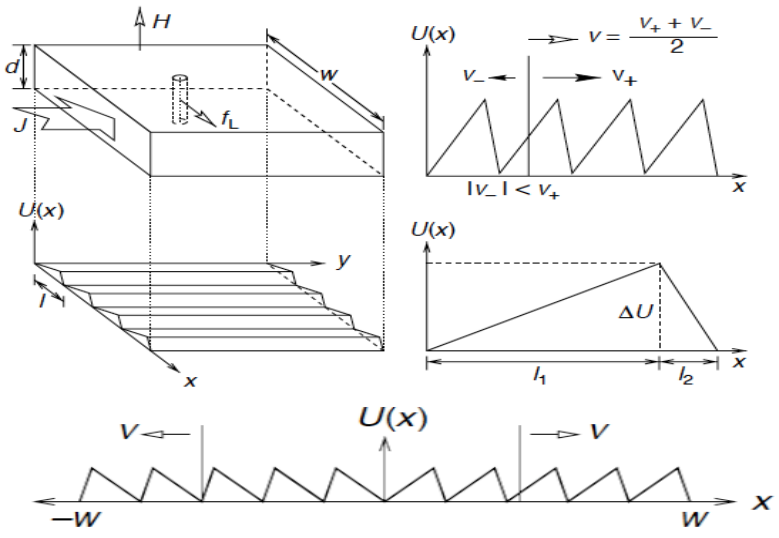

Figure 1.8: A diagram illustrating vortex rectification. Left top: A thin film of type II superconductor penetrated by a magnetic field H. A current density J induces a Lorentz force f_L that moves the vortex in the x direction. Left middle: The superconductor is covered with an array of pinning centres, whose pinning potential $U(x, y) = U(x)$ is shown here. The potential is periodic and asymmetric along the x direction and translationally invariant along the y direction. Right top: The cross-section shows the pinning potential along the x axis as seen by a vortex travelling in that direction. The solid arrows show the vortex velocity v_+ induced by a direct current $+J$ and v_- induced by a reversed current $-J$. The average of the two is the vortex ratchet velocity resulting from an alternating current. Right middle: Parameters characterising a single tooth of the asymmetric potential, see reference [53]. Bottom centre: Two back to back vortices can flush vortices out of a the centre region.

Figure 1.8, and patterned with an asymmetric pinning potential, $U(x, y) = U(x)$ with period l along the x direction and translationally invariant along the y direction, in the presence of a current J along the y direction the vortices move with velocity:

$$v = (f_L + f_{vv} + f_u)/\eta. \tag{1.30}$$

Here, f_L is the Lorentz force, f_{vv} is the repulsive vortex-vortex interaction, $f_u(dU/dx)\dot{x}$ is the force due to the periodic potential and η is the viscous drag coefficient.[53]

When a current flows along the positive y direction, the resultant Lorentz force moves the vortices along the positive x direction $|v_+|$. When the current is reversed the direction of the vortices is also reversed $|v_-|$. However, due to the asymmetric pinning potential $v_+ > |v_-|$. Consequently, when an ac drive is applied to the spatially asymmetric ratchet a net vortex velocity is achieved $v = (v_+ + |v_-|)/2$. Therefore, if two back to back ratchets of this kind are placed about a type II superconductor device, see Figure 1.8 bottom, they can flush vortices away from a site of sensitive measurements.[53]

In section 1.6.1, we describe how a time asymmetric drive can also be used to achieve vortex rectification. These have the advantage of not requiring the construction of an asymmetric spatial geometry. In our own work we investigated how particle size affects rectification by variation of the particle radius. In Chapter Three, we show how this variation affects rectification.

1.5 Absolute Negative Mobility

Another noise induced transport mechanism that we shall have cause to mention in Chapter Two is absolute negative mobility. This is the phenomenon whereby a formerly unperturbed system, in thermal equilibrium, upon application of an external static force F, in a particular direction a, responds with an average particle motion in the opposite direction $-a$ if in addition an ac zero averaged drive is applied. It arises when the magnitude of F is not too large. Moreover, when $F = 0$ no average particle current is present.[115, 116, 117]

Formerly, it was thought that in order to achieve absolute negative mobility finely tailored spatial asymmetry of either the chamber geometry or the nonlinear particle-particle interactions was required.[117] However, a more practical way of achieving absolute negative mobility has been proposed whereby spatial asymmetry has been embedded within the transported particle rather than the confining chamber.[117] This has the advantage of not requiring finely constructed chamber geometries in nanotechnology thus reducing fabrication costs. It also means that this form of absolute negative mobility is more likely to be found in biological systems where cylindrically symmetric channels and elongated particles may be encountered.

With this in mind an overdamped Brownian particle in the shape of an elliptical disk was modelled in the two dimensional channel shown in the inset of Figure 1.9, by a 2D Langevin equation. Both the particle displacement and orientation were noise dependent. The particle was subject to a direct drive F_{dc} and an alternating force F_{ac}, such that its amplitude was characterised by $max|F_{ac}| = F_{dc}$ and its period was given by T_Ω. The chamber geometry was such that $x_L = y_L = 1$ and $\Delta/y \ll 1$. The elliptical particle had semi-major

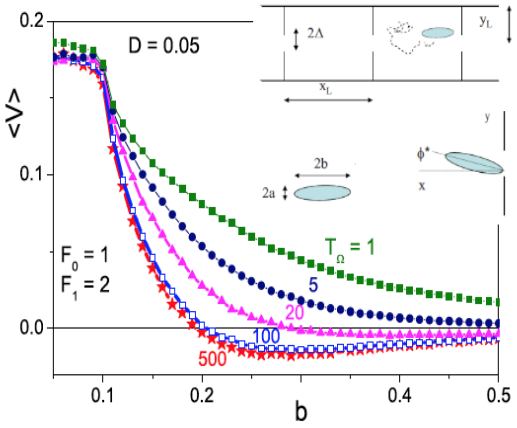

Figure 1.9: The dependence of particle net velocity $\langle v \rangle$ versus semi-major axis b for different values of the F_{ac} drive period T_Ω. F_{ac} had a square waveform with amplitude strength $F_{ac} = 2$, $F_{dc} = 1$, other parameters were $a = 0.05$, $x_L = y_L = 1$ and $\Delta = 0.1$ Inset: The channel where the elliptical particle was confined. The chamber had dimensions $x_L = y_L = 1$ and $\Delta = 0.1$, as we have said. The particle has semi-major axis b and semi-minor axis a. ϕ was the angle between the major axis of the particle and the channel axis as shown. ϕ^* was the values of ϕ such that the elliptical particle could escape the chamber.[117]

axis b and semi-minor axis a, such that $a < \Delta < b$. It had angle ϕ between the major axis and the channel axis. In this regime, it was found in Figure 1.9 main panel, that the net current $\langle v \rangle$ depended on the particle elongation. The net velocity $\langle v \rangle$ changed from positive to negative at a threshold value of b denoted b^* that itself increased with increasing noise intensity D or decreasing T_Ω. This was explained in terms of the value of b relative to the pore width Δ and its angular orientation, see reference [117]. But of relevance here is that this demonstrates once again the importance of the extensive nature of particles in stochastic dynamics and the need to consider the same in the phenomena of geometric stochastic resonance and rectification.

1.6 Stochastic Transport: Applications

Finally in this introductory chapter, we consider some of the many applications of stochastic transport. We limit ourselves to a consideration of the con-

trol of vortices in type II superconductors, bacterial motion and self-propelled particles, and the directed transport of colloids and Janus particles in nanotechnology.

1.6.1 Vortices

Vortices arise when a magnetic field penetrates a type II superconductor film with intensity H between the lower critical field H_{c1} and the upper critical field H_{c2} and produces entities called Abrikosov vortices. Vortex density can be controlled by varying the magnetic field intensity H. Due to vortex-vortex repulsion, the vortices arrange themselves into a vortex lattice with density $\rho \approx H/\Phi_0$, where Φ_0 is the flux quantum. The lattice is usually triangular in arrangement but may include defects or dislocations like crystalline lattices. A local electrical current density I can exert on each fluxon a Lorentz force $\mathbf{F}_L = \Phi_0 \mathbf{I} \times \mathbf{H}/(cH)$ by means of which the vortex motion can be controlled, see Figure 1.10.[26]

Magnetic vortices in type II superconductors can provide experimental verification of stochastic transport models. Moreover the control of vortices in type II superconductors can lead to a new range of technologies referred to as fluxtronics.[26] Abrikosov vortices are inherently quantum entities. However, under most experimental conditions they behave like massless point-like objects and as such they can be modelled by the overdamped Langevin equation.

Vortices can interact with natural inhomogeneities in the crystalline structure of the superconductor or with artificially introduced ones. The arrangement and composition of these pinning centres can affect the thermodynamics and vortex transport properties of the superconductor. Pinning centres oppose vortex motion and consequently determine the critical current below which vortex motion ceases. Pinning centres were initially the result of crystalline defects or impurities in the superconductor, but they were later purposefully introduced to increase the critical current. Ion beam lithography later allowed the construction of sharp confining geometries over a large surface of the superconductor.[26, 51] Matching effects can arise between these pinning centres and the Abrikosov vortex lattice. These arise when the number of vortices and pinning centres are m/n where m and n are integers. The resultant commensuration effects are responsible for a variety of dynamical superconducting states of importance to vortex rectification.[26, 52]

Vortex rectification in a type II superconductor was first demonstrated theoretically when it was shown that an ac electric current applied to a superconductor with an asymmetric array of pinning centres resulted in vortex transport, with a direction determined solely by the asymmetry of the pinning centre pat-

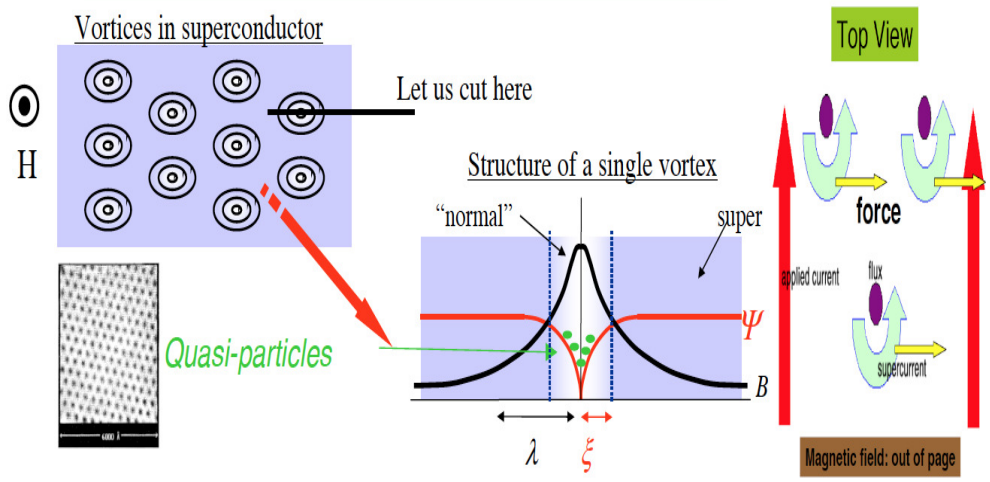

Figure 1.10: Left: Vortices seen from above in a type II superconductor with the magnetic field intensity H passing out of the page towards us. Middle: Cross-section of same showing the structure of a single vortex. λ is the London penetration depth, ξ is the coherence length, B is the magnitude of the magnetic field and Ψ is the modulus of the superconducting order parameter. The labels 'normal' and 'super' identify the normal and superconducting regions of the material. The vortex has a normal core. Right: A representation of how the vortices in a type II superconductor can be directed by means of an applied current. An applied current in the vertical (red arrows) causes the vortices to move in the horizontal direction due to the Lorentz force upon them, (yellow arrows). The purple dots represent the vortex cores and green arrows represent the superconducting current encircling the vortex. Photograph inset left: STM of an Abrikosov flux lattice produced by a 1T magnetic field in $NbSe_2$ at 1.8k, the image is 6000Å across, see reference [130].[50]

tern, see Figure 1.11. The fluxons were treated like massless point-like particles moving along a sawtooth potential. In this setup, it was found that for an appropriate choice of the pinning potential, a rocked ratchet could be used to manipulate single vortices in a superconducting sample under experimentally realisable conditions. This mechanism of fluxon rectification on a ratchet potential had been anticipated by Marchesoni, Savel'ev and Nori.[26, 53, 54, 55]

Fluxon lattice rectification is an inherently 2D process. Devices have been developed that have experimentally demonstrated the control of vortex ratcheting both in the direction parallel (longitudinal rectification) and perpendicular to the applied ac Lorentz force (transverse rectification).[26, 56, 57, 58]

Longitudinal rectification in a 2D array of asymmetric pinning centres was

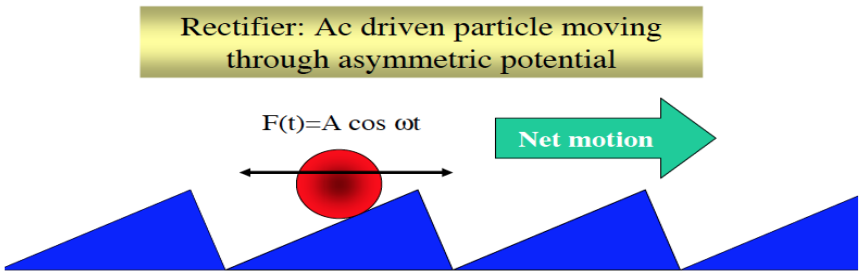

Figure 1.11: A vortex moving through an asymmetric potential and subject to an ac drive achieves net motion in the easy direction, see also Figure 1.8.[50]

experimentally demonstrated when it was shown that under appropriate operating conditions, fluxon rectification was enhanced for Lorentz force amplitudes between the lower and upper critical pinning forces determined by the underlying asymmetric substrate.[26, 59] These lower and upper critical forces were the repinning and depinning forces respectively. Harmonic mixing on a symmetric substrate has also been experimentally demonstrated. A symmetric fluxon lattice was trapped in a triangular array of circular holes playing the role of pinning centres that had been photolithographed onto a $Bi_2Sr_2CaCu_2O_{8+\delta}$ single-crystal thin film by setting the applied magnetic field to the lowest multiple of H_1, where H_1 was the first matching field equal to $H_1 = \Phi_0/a^2$ and Φ_0 was the flux quantum and a was the lattice cell period. This fluxon lattice was then subjected to a biharmonic Lorentz force orientated along the crystallographic axes of the pinning centre lattice. However, the resultant biharmonic mixing could be explained in terms of the 1D reductionist approach.[26, 60]

Transverse fluxon rectification however requires irreducible 2D modelling. Experimental devices capable of transverse rectification can be realised by either varying the orientation of the pinning lattice axes, the symmetry axes of the individual traps (if any) or the direction of the driving current.[26] By these means transverse fluxon rectification has been realised and can be consigned to two main categories, either (i) symmetric arrays of asymmetric traps or (ii) asymmetric arrays of symmetric traps. In the case of (i) symmetric arrays of asymmetric traps, an experimental setup confirmed the numerical simulations by Savel'ev and coworkers, who had predicted that the same device could exhibit either longitudinal or transverse output current depending on the orientation of

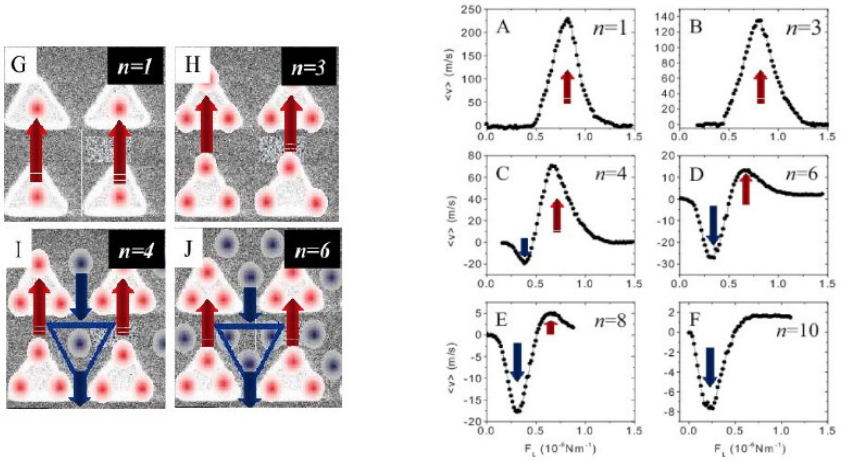

Figure 1.12: Left: A symmetric array of asymmetric triangular pinning centres on the surface of a type II superconductor. The red and blue dots represent pinned and interstitial vortices respectively, while the arrows represent their respective motion due to the Lorentz force upon them from the injected current. Each panel shows the situation for different values of the magnetic field intensity $H(n)$, where n is the number of vortices per unit cell of the device. With increasing $H(n)$ reversible rectification could be achieved. Right: Net velocity $\langle v \rangle$ of vortices versus the amplitude of the ac Lorentz force F_L for different magnetic field intensities $H(n)$. Again the red and blue arrows indicate the region where the net motion is dominated by the pinned or interstitial vortices and again we see reversible rectification. For more information see [26, 62]

the ac drive with respect to the pinning lattice axes.[63, 26] In the longitudinal ratchet configuration a sinusoidal driving current was applied perpendicular to the axis of reflection symmetry of the pinning centres, (x axis), and the output voltage was recorded in the same direction. The resulting Lorentz force induced vortex motion parallel to the y axis corresponding to a voltage drop along the x axis. For transverse rectification the axes of the current injection and voltage drop were reversed. More interesting still in this experimental set up was the reversible rectification achievable upon changing the magnetic field intensity H and due to the behaviour of the pinned vortices (inside nano-fabricated triangles) and interstitial vortices (between triangles) under the influence of the injected current, see Figure 1.12 and references [61, 62].[26, 61, 62, 63]

Rectification has also been demonstrated in the absence of a ratchet substrate in a layered superconductor. In such materials an externally applied

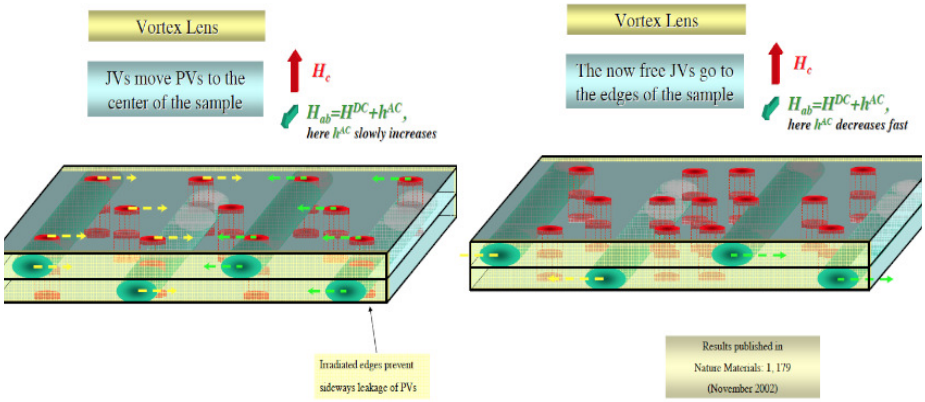

Figure 1.13: A crossing vortex lattice is constructed by two magnetic field penetrating the layered superconductor at right angles to one another. The resulting Josephson vortices (JVs) are weakly pinned and can be driven along by an in-plane magnetic field $H_{\parallel}$ or an applied electric current I_x along the c axis, (vertical axis here). A time asymmetric oscillation of in-plane magnetic field drives the JVs along which drag the pancake vortices (PVs) after them, resulting in a net motion of the PVs. The cycle can be repeated resulting in vortex lensing. Vortex antilensing can also be achieved. The device acts like a ratchet but without an asymmetric substrate. Consequently the technique can be used to enhance the sensitivity of SQUID magnetometers and other superconductor based devices.[26, 50, 64, 108, 109]

magnetic field created Josephson vortices confined along the ab plane and pancake vortices along the c axes. These two types of vortices attract one another and by externally moving the Josephson vortices the pancake vortices can be dragged along after them. A time asymmetric ac drive produces rectification of both components of the binary mixture which can be controlled by means of the ac drive parameters, see Figure 1.13. Cole and coworkers experimentally demonstrated that the asymmetrical dragging of the Josephson vortices resulted in lensing and antilensing of the pancake vortices.[26, 50, 108, 109] This type of rectification has the advantage of simplicity, it requires no spatial asymmetry of pinning centres just the tuning of vortex motion by changing the parameters of the injection current and so it lends itself to experimental setup and fabrication alike.[26, 50, 64]

1.6.2 Colloids

A colloid, or colloidal suspension, consists of a dispersed phase of insoluble particles on the range of 1nm - 1 μm suspended in a continuous phase the medium.[24] Colloids are characterised by a dispersed phase that does not settle out of the continuous phase in an appreciable length of time, unlike a solute in a solvent. Colloids include gels, sols and emulsions. Their uses range from dyes, detergents and polymers, to drugs and drug delivery systems such as the Janus particles we shall consider shortly.[24]

Colloids are subject to stochastic dynamics and as such offer an additional method of experimental verification of simulations in confined geometries such as corrugated channels. Many of the forces that control the structure and dynamics of molecules, such as electrostatic forces also control the structure and dynamics of colloidal suspensions.[25, 26] On the micrometer scale colloids are large enough to be studied by optical microscopy. Colloidal systems have relatively slow dynamics, consequently they can be tracked at the single particle level by video microscopy.[25, 27] External magnetic fields or optical tweezers can also be applied to colloidal systems to confine the particles in a regular lattice akin to Brownian particles in a corrugated channel. An array of optical tweezers, each acting as an optical trap on the diffusing colloidal particles has been used to study hydrodynamic drag, enhancement of diffusion under an external force and the sorting of particles based on size difference.[25, 28, 29, 30] Phase transitions in soft matter has also been studied in real time using optical techniques.[25]

Colloidal suspensions have been used to study barrier-crossing as occurs in cell membranes and interstitial spaces. The system allows the simultaneous tracking of particle motion and measurement of the energy landscape. This has enabled the study of diffusion over energy landscapes under a constant force and anomalous diffusion in random fields with heterogeneous energy barriers.[25]

In a recent experiment a tilted two-layer colloidal system was set up to study the dynamics of force-assisted barrier-crossing over a periodic potential.[25, 31] The apparatus consisted of a bottom layer of colloidal spheres forming a fixed crystalline pattern on a glass substrate. This served as a periodic potential. The corrugated surface provided a gravitational potential field for the top layer of diffusing particles. The apparatus was tilted at an angle with respect to the vertical and so a tangential component of the gravitational force F was applied to the diffusing particles. The mean drift velocity and diffusion coefficient of the particles were then measured as a function of the tangential component of the gravitational force and energy barrier height for comparison with stochastic dynamics models of forced barrier crossing.

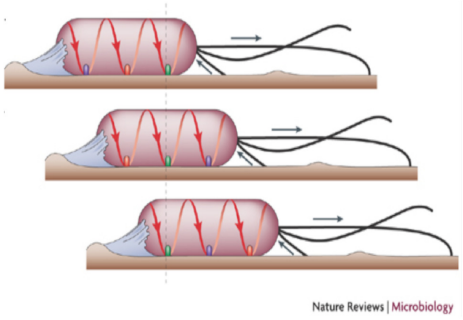

Figure 1.14: Twitching motility: Pili (black cords) are extended from the periphery of the bacterium and adhere to the surface. The bacterium then draws itself over the surface by pili retraction, (right pointing arrows indicate pili extension, left pointing arrows indicate pili retraction). This cycle of pili extension, adherence and retraction is repeated to draw the bacterium over the surface. From reference [36] with slight modification.

Colloidal systems have also been used to demonstrate rectification in ratchet potentials. A colloidal suspension was exposed to a sawtooth dielectric potential which was turned on and off periodically. It was known that particles subjected to an asymmetric periodic potential would display net directional motion even if the space averaged force was zero. The particles exhibited a net motion with a velocity that depended on their size. This had applications for particle separation processes for objects on the size range $0.1 - 5.0\mu$m. This includes biological molecules, viruses, cells and chromosomes.[32]

1.6.3 Intermission: Bacteria

For inspiration on methods of self-propulsion on the nanoscale researchers have turned to the bacterial world (approximate scale 10^{-5}m) where several mechanisms of self-propulsion are in evidence including: flagellar motion, tumbling, screwing, gliding motility and twitching.[34] The latter involves the extension of pili from the bacterium followed by their retraction as the bacterium draws itself through the medium see Figure 1.14.[33, 34, 35, 36, 37] This is not unlike the radial oscillation of the self-propelled biological particles we consider in Chapter Three, where the particle radius was composed of a fixed internal component of radius $R_1 = a$ and an oscillating external component of radius $R_2 = b|\cos\omega t|$, as the oscillation in particle radius affected particle-boundary interactions and passage times.

Bacterial motion is governed by the scallop theorem which affects self-propulsion at low Reynolds number.[33, 38] The Reynolds number is a dimensionless number that compares the inertial and viscous forces in a medium and

is given by: $R = av\rho/\eta$, where a is the body length of the bacterium, v its speed, ρ the density of the surrounding medium and η its viscosity. The scallop theorem states that any sequence of body configurations intended to produce motion that retraces itself to complete a cycle results in no net motion.[38] Thus bacteria must break spatial symmetry of motion in order to produce a net displacement. Two means by which they accomplish this using the flagellar motion mentioned above involve either a corkscrew or flexible oar motion.[33] It is to be expected therefore that self-propelled particles must also contend with the proscriptions of the scallop theorem in order to achieve net motion.[38]

However, when one attempts to implement these methods of bacterial self-propulsion on the molecular level (approximately 10^{-8}m and smaller), one encounters an additional problem: diffusion caused by thermal noise (Brownian motion) swamps self-propelled motion.[33] In biology this is solved by constraining molecular motion to a one-dimensional track composed of a periodic series of wells and barriers. The energy barriers restrict the diffusion and the thermal noise then plays a constructive role by enabling the molecules to escape from one well to the next. The energy barriers or wells can be periodically raised and lowered via an energy input such as from an external time-dependent modulation or a non-equilibrium source. Thus directed motion of molecules can still be achieved on the molecular level even in the presence of thermal noise. Indeed, as we shall show in Chapter Three it can be enhanced still further if these molecules have an element of self-propulsion.

1.6.4 Microswimmers

Interest in particle shape and its effect upon stochastic transport is increasing in part due to the potential applications of Janus particles. These particles are nano-particles composed of two or more different surfaces whose individual physical and/or chemical properties are distinct and in consequence interact differently with their surrounding medium.[39] Their asymmetry of design gives Janus particles unique properties of interaction and a wide variety of potential future applications. These applications include: stabilisation of liquid/liquid and liquid/gas interfaces, nano-probes,[40, 41] biosensors,[42] drug delivery, 'lab on a chip' devices, tailored substrate wettability,[43] and programmable nanostructures capable of self-assembly and reconfiguration, to name but a few.[39]

Not content with prospects for directed transport on the nanoscale by means of rectification, ANM or gSR however, researchers are investigating the additional possibility of self-propelled particles or micro swimmers, as they have become known, which have lately come to include self propelled Janus particles. These particles could fulfil the same role of cargo transport and delivery in

'lab on chip' and drug delivery systems as played by some proteins in biological systems.[39, 44] One means by which this self-propulsion has been achieved is the catalytic degradation of H_2O_2, asymmetrically distributed over the Janus particle surface to release O_2 and propel the particle forward.[45, 46, 47, 48, 49] However, some propulsion is lost to simple particle rotation. Propulsion by such means is further limited by reactant concentrations and an improved method would require reactant replenishment or an external energy source. Nevertheless, self-propelled Janus particles would have an additional means of controllability, further enhancing their utility. Finally, it should be mentioned that in the context of the present work we use the term *active particles* to refer to those particles that actively participate in their own motion.

In this introductory chapter to the thesis, we have defined and described stochastic transport phenomena necessary to the understanding of the research conducted in Chapters Two and Three. These stochastic phenomena included: stochastic resonance, both energetic, entropic and geometric, rectification and absolute negative mobility. We have described a model of stochastic transport using the overdamped Langevin equation. Furthermore, we have dealt with the modelling of stochastic transport in both 1D and higher. With regard to the 1D model, we have considered its limitations and the consequent irreducible nature of some stochastic transport phenomena particularly geometric stochastic resonance. Finally, we have considered some of the many applications of stochastic transport to vortices in type II superconductors, colloids and microswimmers.

Having thus reviewed the background material necessary to the understanding of the research conducted and described in Chapters Two and Three and reviewed the research that motivated that work, we hope that we have set geometric stochastic resonance and rectification in the broader context of stochastic transport. We hope that we have highlighted the limitations of modelling stochastic transport in one dimension and summarised some of the practical applications of the control of stochastic transport. We also hope that we have shown how noise is integral to stochastic transport and that much effort is being expended in understanding how it can be put to constructive use within systems.

Chapter 2

Geometric Stochastic Resonance

In Chapter Two we describe our research related to the geometric stochastic resonance of Brownian particles in a double cavity in Section 2.1 and that related to the synchronisation of geometric stochastic resonance by a bi-harmonic drive in Section 2.2.

In our first project, described in Section 2.1, the geometric stochastic resonance of particles diffusing across a porous inter-cavity membrane and subject to periodic driving forces was investigated and characterised as a synchronisation process. Non-interacting particle currents were driven through a symmetric membrane pore either parallel or perpendicular to the membrane. Subsequently, harmonic mixing spectral current components were generated by the combined action of parallel and perpendicular drives. The role of particle repulsion in controlling the stochastic dynamics was also investigated with potential applications to the transport of colloids and biological molecules through narrow pores.[1]

In our second project, described in Section 2.2, the stochastic dynamics of an elliptical particle were simulated using the Langevin equation. The particle was driven by both a low and high frequency harmonic drive across the porous membrane that divided the chamber. It was observed that the particle oscillates out of phase with the low frequency drive. This effect was attributed to the absolute negative particle mobility. It was also observed that the magnitude of this out-of-phase stochastic resonance depended upon how the combined action of the driving forces and noise fluctuations affected the particle orientation, and was thereby shown to be sensitive to the particle shape. This emphasises

the importance of particle geometry, in addition to chamber geometry, to the mechanism of geometric stochastic resonance.[2]

2.1 Geometric Stochastic Resonance in a Double Cavity

As we pointed out in Chapter One, stochastic resonance research initially focused on systems with purely energetic potentials either continuous or discrete in nature.[1][1, 77, 78] However, it was later realised that in soft condensed matter and many biological systems, particles are often confined to constrained geometries, such as cavities, pores, interstices, or channels, whose size and shape can affect the mechanism of stochastic resonance.[1, 13, 20, 26, 81] We pointed out in Section 1.3.2 that such smooth confining geometries can be modelled as entropic, noise or temperature dependent, potentials which are as capable of influencing the system response as an external driving force.[1, 4, 11, 79, 80]

A different situation arises however in the case of more sharply confining geometries. Research has shown that a Brownian particle confined to two distinct cavities separated by a porous membrane underwent stochastic resonance in the presence of an ac driving force perpendicular to the membrane.[1, 66] In contrast to ordinary stochastic resonance, optimal synchronisation between the driving force and the particle oscillations occurred even in the absence of a bistable energetic or entropic effective potential for an appropriate noise level.[1, 20, 77, 78] However, this form of stochastic resonance requires extremely sharp confining geometries, in higher dimensions, to separate the two cavities. Moreover, the magnitude and conditions of this form of stochastic resonance effect are sensitive to both the geometry of the cavities and the structure of the pores.[1]

Geometric stochastic resonance is distinct from entropic stochastic resonance where the Brownian particle can switch between cavities only by overcoming the entropic barrier determined by the geometric constraint associated with the smooth pore.[1, 20] In the absence of an energetic barrier, the entropic barrier can determine the magnitude of the stochastic resonance effect that occurs when the periodic driving force drives the particle across the pore. Although, in the original research on entropic stochastic resonance, an interplay between the entropic and energetic barriers rather than a mere entropic effect was suggested.[1, 20]

Geometric stochastic resonance is a unique form of driven Brownian motion in septate channels.[1, 19, 82, 83, 84, 85, 117] In these septate channels,

[1]The research described here in Section 2.1 is published in: Ghosh, P.K. Glavey, R. Marchesoni, F. Savel'ev, S.E. Nori, F. (2011) 'Geometric stochastic resonance in a double cavity', *Physical Review E*, 84, 011109.

the chambers are separated by partition walls of zero thickness and consequently the pores piercing the centre of these partitions can be modelled as structureless holes. These septate channels cannot be analysed in terms of the 1D reductionist approach of Chapter One as entropic channels, because the geometry of the pores is too sharp to be accurately modelled by the Fick-Jacobs approximation.[1, 4, 11, 13, 79, 80] Instead, they must be modelled and analysed by an integration of the relevant Langevin equation in two or higher dimensions. However these sharp pore geometries do enhance most noise controlled transport mechanisms, making them suitable to experimental verification.[1, 26, 81]

In the model presented here, we considered a two dimensional geometry. This was based upon the ongoing research in vortex superconductor devices. As we mentioned in Chapter One, these devices have numerous technological applications, including flux qubits in potential quantum computers, superconducting quantum interference devices and (SQUIDs).[1, 60, 64, 119, 120, 121, 122, 123, 124] Ion beam lithography has enabled the construction of almost any geometry upon the surface of a type II superconductor. Consequently, superconducting samples with two vortex containing boxes connected by a thin pore of almost any geometry can easily be fabricated. Vortices can be trapped within these boxes with binding energies on the order of $\Phi_0^2 L_t/\lambda^2$, where Φ_0 is the magnetic flux quantum, λ is the London penetration depth, and L_t is the depth of the vortex traps. These vortices repel one another via a logarithmic pair potential. The vortex density, $n = H/\Phi_0$, is controlled by the intensity, H, of the applied magnetic field. In the dilute limit, $H \lesssim \Phi_0/\lambda^2$, the vortex-vortex interactions become negligible and the transport properties of an individual trapped vortex are not hidden by many body effects. In terms of experimental setup, periodic driving forces and noise sources can be implemented as Lorentz forces generated by independent electric currents injected into the sample parallel and perpendicular to the pore axis. In this way stochastic resonance can be detected under experimental conditions using only the applied current sources. In particular, the noise parameter can be varied independently of the constant operating sample temperature.[1]

2.1.1 Model

In this model, we simulated overdamped Brownian particles freely diffusing in a two dimensional suspension fluid contained in two symmetric chambers with reflecting walls connected by a narrow pore of width Δ, as shown in Figure 2.1(a). The overdamped dynamics of the particles were modelled by the Langevin equation 2.1.

$$\frac{d\vec{r}}{dt} = -\vec{A}(t) + \sqrt{D}\vec{\xi}(t). \tag{2.1}$$

Here $\vec{A} = (A_x, A_y)$ were the x, y components of the driving force and $\vec{\xi}(t) = [\xi_x(t), \xi_y(t)]$ were zero mean Gaussian white noises with autocorrelation functions $\langle \xi_i(t), \xi_j(t') \rangle = 2\delta_{ij}\delta(t - t')$ with $i, j = x, y$. Equation 2.1 was numerically integrated by a Milstein algorithm. Stochastic averages were taken as ensemble averages over 10^6 trajectories with random initial conditions. Transient effects were estimated and subtracted.[1]

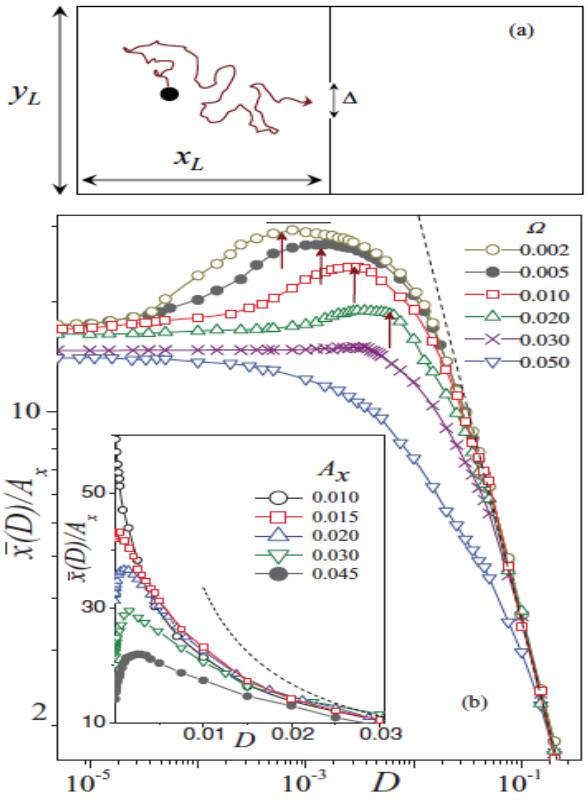

Figure 2.1: (a) A Brownian particle confined in a two dimensional box consisting of two chambers separated by a partition wall with a pore of width Δ at its centre. The chamber had dimensions $x_L = y_L = 1$. (b) A graph demonstrating geometric stochastic resonance showing $\bar{x}(D)$ versus D for different values of Ω at $A_x = 0.045$, (main panel), and different values of A_x at $\Omega = 0.01$, (inset). The other parameters were $x_L = y_L = 1$ and $\Delta = 0.1$. The inset shows predictions for the stochastic resonance peak position D_{max} (vertical arrows) and height $\bar{x}(D_{max})$ (top line). The dashed line in both graphs represents the decay law $\bar{x}(D \to \infty)$.[1]

In the presence of a longitudinal ac driving force directed along the x axis $A_x(t) = A_x \cos(\Omega t)$, the Brownian particle trajectories embedded a persistent harmonic component $\bar{x}(D)cos[\Omega t - \phi(D)]$. The resultant amplitude, $\bar{x}$ was plotted versus D in Figure 2.1(b).[1, 66]

The three main characteristics of geometric stochastic resonance are: (i)

$\bar{x}(D)$ reaches a maximum for an appropriate noise intensity D_{max} with an upper bound determined by the inequality 2.2.

$$\bar{x}(D_{max}) \leq \frac{4}{\pi} x_L. \tag{2.2}$$

An estimate of this D_{max} was obtained by matching the half drive period with the mean first escape time from one chamber to the next at $A_x = 0, \tau_\Delta(D)$, that is:

$$\tau_\Delta(D_{max}) = \frac{T_\Omega}{2} \equiv \frac{\pi}{\Omega} \tag{2.3}$$

The first exit time, $\tau_\Delta(D)$ was inversely proportional to the noise intensity D and strongly depended upon the pore width Δ. For narrow pore widths, $\tau_\Delta(D)$ diverged with y_L/Δ, that is, proportional to $\ln(y_L/\Delta)$, where y_L was the chamber width, see Figure 2.1. Therefore, D_{max} was proportional to Ω.[1, 2, 66, 84, 85]

(ii) Stochastic resonance is restricted to $A_x > A_c$ or $\Omega < \Omega_c$ as a result of the geometric condition that,

$$\frac{A_x}{\Omega} \geq \frac{4}{\pi} x_L, \tag{2.4}$$

requiring that, in the absence of noise, the ac driven particle should hit the walls of the chamber twice per period of the driving force. Here x_L is the chamber length along the x axis, see Figure 2.1. This is an important distinction from ordinary stochastic resonance, where no such onset thresholds exists in the drive parameters space.[1, 77, 78]

(iii) The amplitude $\bar{x}(D)$ obeys the approximate stochastic resonance curve,

$$\bar{x}(D) = \frac{\bar{x}_0(D)}{\sqrt{1 + [\Omega \tau_\Delta(D)]^2}}, \tag{2.5}$$

where

$$\bar{x}_0(D) = \frac{A_x x_L / D}{\tanh(A_x x_L / D)} \tag{2.6}$$

is the amplitude of the $\langle x(t) \rangle$ oscillations in the adiabatic limit $\Omega \to 0$. As a consequence of this, for large noise, $\bar{x}(D) \propto 1/D$.[1]

Equation 2.3 is the geometric stochastic resonance equivalent of the standard stochastic resonance condition, where in the absence of an energetic barrier, the Arrhenius time is replaced by an appropriate diffusion time across the inter-cavity pore.[1, 77, 78, 87, 88] From equation 2.6, it can be seen that for weak noise and low drive frequencies, $A_x(t)$ presses the particle against the walls of the chamber opposite the partition wall, and, as a result, the average particle displacement $\langle x(t) \rangle$ approaches a square wave form with amplitude x_L. Then

the amplitude of the Fourier component of $\langle x(t) \rangle$ with angular frequency Ω is $4x_L/\pi$. This explains the inequalities of equations 2.2, 2.4, where A_x/W is the driven oscillation amplitude of an unconstrained Brownian particle. The upper bound of equation 2.2 holds for vanishingly low Ω, see Figure 2.1(b). For stronger noise but low drive frequencies, $\bar{x}_0(D)$ tends to $A_x\tau_x$, where $\tau_x = x_L^2/3D$ is the longitudinal diffusion time across a cavity compartment. The pore effectively suppresses the particle oscillations with damping constant $\tau_\Delta(D)^{-1}$ only at relatively high drive frequencies as can be seen from equation 2.5. These analytical results agree well with the simulations.[1, 66]

2.1.2 Synchronisation Mechanisms

The evidence for geometric stochastic resonance presented in Section 2.1.1 focused on the D dependence of the harmonic component of the $\langle x(t) \rangle$ with driving frequency Ω.[1, 66]

However, an alternative description of the resonance mechanism can be based upon the synchronisation characterisation of the stochastic resonance phenomenon.[1, 92, 93] In this description, one considers the residence times T of the Brownian particle in either cavity, due to the mirror symmetry of the process with respect to the cavity partition either cavity will do. Their distribution densities $N(T)$ exhibit a prominent peak structure and a resonating dependence upon D and T.[1]

Longitudinal Drive

We first considered the case of longitudinal drives $A_y = 0$. In Figure 2.2(a), we plotted $N(T)$ for different values of Ω at constant D. From the graph it could be seen that the $N(T)$ peaks were centred around

$$T_n = \left(n - \frac{1}{2}\right) T_\Omega, \qquad n = 1, 2, 3, ... \quad . \tag{2.7}$$

This was due to the fact that the left to right pore crossings were more likely to occur when the longitudinal ac force $A_x(t)$ pointed from the right to the left and vice versa. This synchronisation mechanism has been discussed in the stochastic resonance literature.[77, 78] The numerical analysis, shown in Figure 2.2(a) for $n = 1$, proves that the area enclosed beneath, the nth distribution peak increases with Ω up to an optimal value $\Omega = \Omega_n$, and then decreases for higher Ω. The optimal value Ω_n is determined by the optimal synchronisation condition.[1, 92, 93]

$$\left(n - \frac{1}{2}\right) T_\Omega = \tau_\Delta(D), \qquad n = 1, 2, 3, ... \quad . \tag{2.8}$$

For $n = 1$, this equality coincides with the spectral stochastic resonance condition of equation 2.3. This proves that the first peak can be enhanced to a maximum by acting either upon T_Ω or upon τ_Δ, this conclusion actually applies to all the peaks. This proves that geometric stochastic resonance is itself a genuine form of resonance.[1, 92, 93]

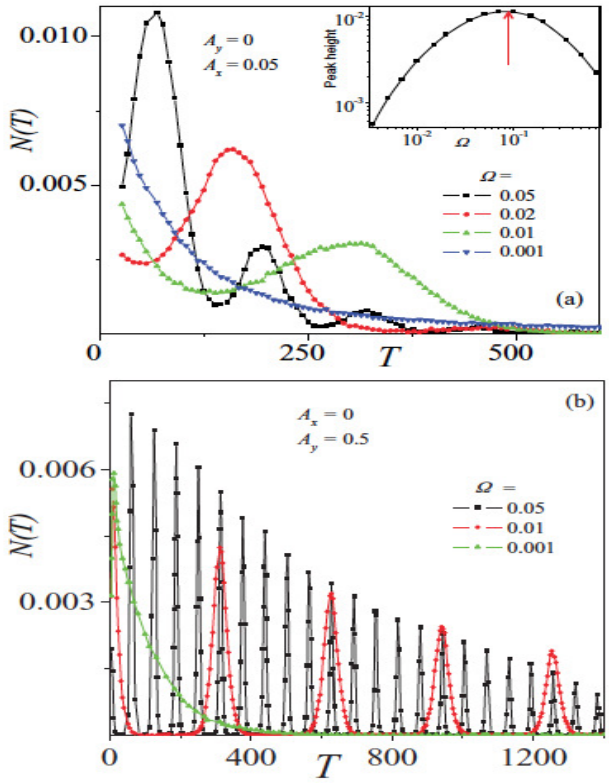

Figure 2.2: The distribution density of residence times for different periods $T_\Omega = 2\pi/\Omega$ (in the legends) of the (a) longitudinal drive with $A_x = 0.05$ and (b) transverse drive with $A_y = 0.5$. The cavity dimensions were as in Figure 2.1 and $D = 0.015$. The inset in (a) shows the height of the first peak $n = 1$ versus Ω. The vertical arrow denotes the resonant Ω value predicted in equation 2.8 with τ_Δ given in references [84, 85].[1]

Transverse Drive

We then considered the case of transverse drives $A_x = 0$. A drive parallel to the wall of the cavity in Figure 2.1(a) cannot break the mirror symmetry of the system in the x direction. However, the transverse drive affects the diffusion through the pore because it presses the Brownian particle against the horizontal walls, twice per driving period. When the particle is pressed against the top

and bottom walls of the cavity which are symmetrically placed with respect to the pore, the particle is less likely to escape the side of the cavity into the adjoining chamber. It is more likely to do so however as A_y reverses sign, twice per period. Therefore, it is to be expected that $N(T)$ develops a denser peak structure with

$$T_n = \frac{n}{2} T_\Omega, \qquad n = 1, 2, 3, ..., \tag{2.9}$$

as shown in Figure 2.2(b). Similar to Figure 2.2(a). the distribution peaks become sharper for an optimal value of Ω. Numerical analysis shows that such an optimal synchronisation also occurs under the resonance condition of equation 2.8, but with the difference that $\tau_\Delta(D)$ stays for the transverse diffusion time $\tau_y = y_L^2/3D$. Although the right and left flows through the pore are modulated in time, in the presence of a transverse drive $A_y(t)$, no geometric stochastic resonance can occur because of the mirror symmetry of the longitudinal motion.[1]

2.1.3 Harmonic Mixing

The spectral characterisation of geometric stochastic resonance, as described in Section 2.1.1, can provide more insight into the resonant transport mechanism in a partitioned cavity. The power spectral density of $x(t)$, $S(\omega)$, can be taken and the δ-like spike $(\pi/2)\bar{x}^2(D)\delta(\omega - \Omega))$ can be evaluated, corresponding to the harmonic component of $\langle x(t) \rangle$ with frequency Ω.[1, 66] As shown in Figure 2.3(a), $S(\omega)$ developed a series of spectral spikes at

$$\omega_n = (2n - 1)\Omega, \qquad n = 1, 2, 3, ... \quad . \tag{2.10}$$

From previous research on stochastic resonance, it is known that the even harmonics of the driving frequency are absent due to the $x \to -x$ symmetry of the 2D Langevin equation 2.1.[1, 77, 78] However, as mentioned in Section 2.1.2 stochastic resonance does not occur in the presence of transverse drives. The power spectral density for $A_x = 0$ and $A_y \neq 0$ displayed in Figure 2.3(a), showed no resonance spike.[1]

In Figure 2.3(b) the Brownian particle was subjected to both longitudinal and transverse drives simultaneously. The nonlinearity of the longitudinal and transverse drives causes a mixing between them, a phenomenon called harmonic mixing.[1]

The three key ingredients for harmonic mixing to occur in a one dimensional nonlinear system are (i) nonlinearity of the driven process, (ii) a combination of at least two harmonic drives with angular frequencies Ω_1 and Ω_2 respectively, and (iii), commensuration of the driving frequencies, that is, $\Omega_1/\Omega_2 = p/q$

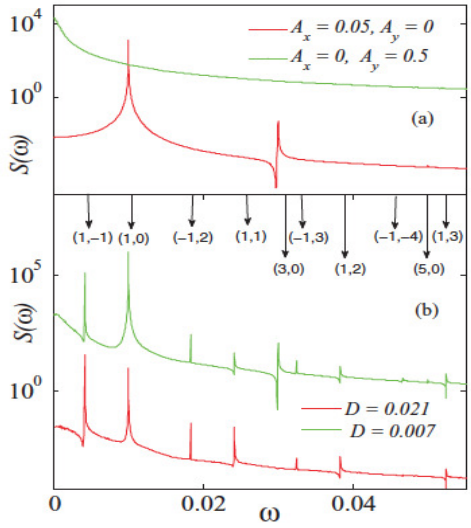

Figure 2.3: The graph shows the spectral density of the coordinate $x(t)$ for two different noise intensities D and (a) either a longitudinal or a transverse drive, (b) a combination of longitudinal and transverse drives. The drive parameters were $A_x = 0.05, A_y = 0.5, \Omega = 0.01$ and $\Omega = \Omega/\sqrt{2}$. The harmonic mixing resonances are indicated by down pointing arrows with the relevant indices (m, n).[1]

where p *and* q are relative prime numbers. With these key ingredients present, the system response to the combination of external drives develops a hierarchy of harmonics at

$$\omega_{m,n} = m\Omega_1 + n\Omega_2 \qquad m, n = 0, \pm 1, \pm 2, \ldots \quad . \tag{2.11}$$

Dynamical symmetries particular to the system under study can lead to the suppression of subsets of these harmonics $\omega_{m,n}$.[1, 125, 126, 127, 128]

However, the system modelled here was two dimensional, so harmonic mixing could occur for any ratio of the driving frequencies. In our simulations, we employed orthogonal harmonic drives $A_x(t)$ and $A_y(t)$ with incommensurate frequencies Ω_x and Ω_y respectively. From Section 2.1.2, it is known that the longitudinal flows driven solely by the transverse drive can only resonate at the even harmonics of Ω_y, namely, for $\omega = 2n\Omega_y, n = 1, 2, 3, \ldots$. This is an effect caused by the mirror symmetry of the cavity with respect to the horizontal axis passing through the centre of the pore. Moreover, the mirror symmetry of the cavity with respect to the walls of the chamber restricts the periodic components of $\langle x(t) \rangle$ to the *odd* harmonics of $A_x(t)$, that is to, $\omega = (2n-1)\Omega_x, n = 1, 2, 3, \ldots$.[1]

In conclusion, the harmonic mixing spectrum of the longitudinal flow through the cavity pore was expected to be

$$\omega_{m,n} = m\Omega_x + 2n\Omega_y, \tag{2.12}$$

with $m = \pm 1, \pm 3, \pm 5, ...$(odd) and n=0,$\pm 1, \pm 2, ...$ and with no commensuration condition of the ratio Ω_x/Ω_y. This is confirmed by the power spectral distribution curves plotted in Figure 2.3(b). Ω_x/Ω_y is an irrational number, however, all spectral peaks detected could be identified by a pair of indices (m, n) according to equation 2.12.[1]

The practical application of the harmonic mixing of longitudinal and transverse drives is that, while the time modulation introduced by the harmonic signal $A_y(t)$ alone could not be picked up by the longitudinal current across the pore, the addition of a small longitudinal signal made $A_y(t)$ detectable. Moreover, the mixing spikes with $n, m \neq 0$ is not necessarily small with respect to the harmonics of the longitudinal signal $n = 0$. In fact, all power spectral distributions spikes $S(\omega_{m,n})$ show a unique stochastic resonance dependence on the noise intensity. For example, in Figure 2.4, the harmonic mixing harmonics $(-1, 1)$ overshoots the fundamental component $(1, 0)$, for an appropriate range of D.

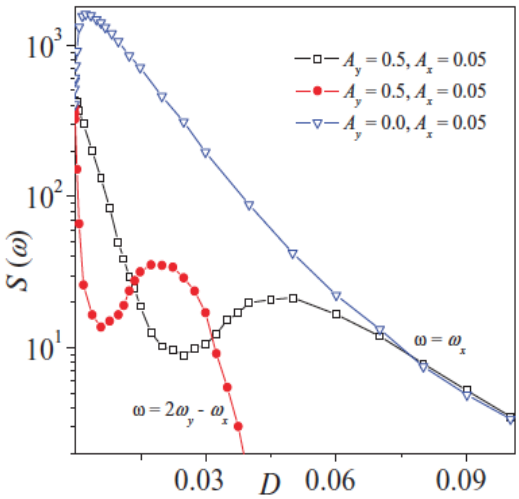

Figure 2.4: The graph shows the resonant behaviour of the two lowest order harmonic mixing components $(1, 0), (-1, 1)$. For comparison, $S(\omega_{1,0})$ is shown also for $(A_x, A_y) = (0.005, 0)$. All other simulation parameters were as in Figure 2.3(b).[1]

2.1.4 Particle Interaction

To better understand the effect of the confining geometry upon the pore crossing mechanism, we also investigated the role of particle interactions. In our simulations, we assumed that the N Brownian particles were randomly distributed between the two chambers of the system and that they repelled one another through the standard vortex-vortex interaction:

$$f_{i,j} = \frac{\alpha}{|\vec{r}_i - \vec{r}_j|}, \tag{2.13}$$

where $i, j = 1, 2, ...,$N i $\neq j$. The situation modelled here is common in biological systems, where constrained geometries may accommodate controllable populations of suspended particles. The exact form of vortex-vortex interaction $f_{i,j}$ is not relevant. What is important however is the dependence of the geometric stochastic resonance upon the parameters of particle concentration N and coupling α of the system of interacting particles.[1, 4, 11, 66, 79, 80, 82, 83, 89, 129]

We considered the geometric stochastic resonance model described in Section 2.1.1, with a longitudinal harmonic drive $A_x(t)$ of fixed angular frequency Ω_x. To account for interactions, we calculated $\bar{x}(D)$ numerically as $\bar{x}(D) = \sqrt{\bar{x}_C^2 + \bar{x}_S^2}$, where

$$\bar{x}_C(D) = \frac{1}{N t_{max}} \sum_i \int_0^{t_{max}} x_i(t) \cos(\Omega_x t) dt, \tag{2.14}$$

$$\bar{x}_S(D) = \frac{1}{N t_{max}} \sum_i \int_0^{t_{max}} x_i(t) \sin(\Omega_x t) dt, \tag{2.15}$$

integrations were carried out over the time interval $(0, t_{max})$ and summations were taken over all the particles. This was equivalent to determining the amplitude of the Ω_x component for the ensemble mean trajectories.[1]

In Figure 2.5 we plotted the graphs $\bar{x}(D)$ for low α in panel (a) and for high α in panel (b), increasing particle concentrations. For low α, increasing the value of N was equivalent to reducing the cavity volume available to the individual Brownian particles. Furthermore, when the particle coupling was relatively weak, the particle interactions exerted only a mean field on the pore crossing. Consequently, in the low coupling regime, it was expected that the stochastic resonance noise intensity D_{max} of equation 2.3 weakly depended on N, whereas, the height of the stochastic resonance peak, equation 2.2, decreased with rising N. This is in good qualitative agreement with the results of Figure 2.5(a). The curve with $N = 1$ is an exception, as it lies beneath the curve for $N = 2$ and peaks at a higher D. All the other curves are centred around the same D_{max}, with their maxima slowly decreasing for increasing N for $N > 2$. In fact, when

passing from $N = 1$ to $N = 2$, pair repulsion actually makes pore crossing more effective than for a single particle. However, this effect becomes negligible when adding one particle for larger N values.[1]

As shown in Figure 2.5, for large α, the vortex-vortex repulsion became so strong that pair crossings were rare. Particles could then only switch cavity by pumping more noise into the system. This meant that the stochastic resonance peaks shifted to higher D_{max} for larger particle concentrations. However, for very large N, the harmonic component of $\langle x(t) \rangle$ was suppressed independent of the value of α.[1]

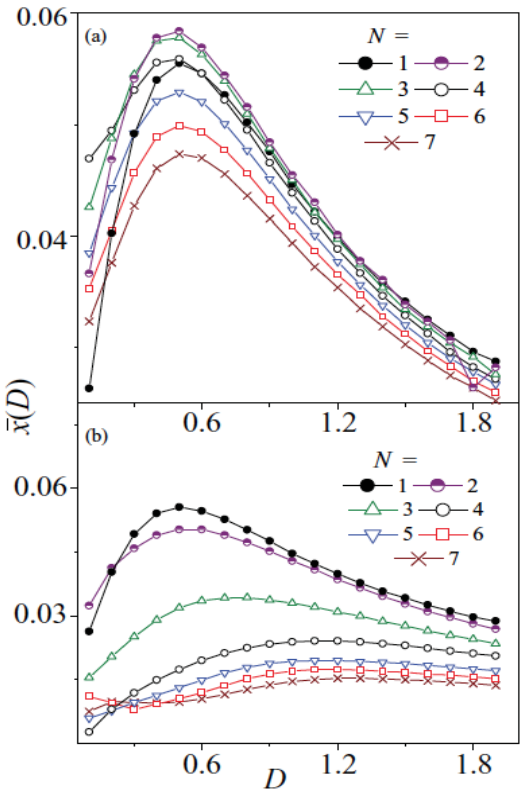

Figure 2.5: The graph shows geometric stochastic resonance for interacting particles, $\bar{x}(D)$ versus D for the double cavity shown in Figure 2.1 for N identical particles repelling one another via the pair interaction force of equation 2.13 with $\alpha = 1$ (a), and $\alpha = 6$ (b). The drive parameters were $A_x = 1, A_y = 0$ and $\Omega = 0.01$.[1]

The α dependence of the driven particle flow across the pore was further illustrated by Figure 2.6 for $N = 2$ and $N = 3$. The curves for low noise, $D < D_{max}$ for $\alpha = 0$, show that, in the absence of interactions, pore crossing happened with a time constant much larger than the half drive period, see equation 2.3. When the particle interaction was switched on the free volume

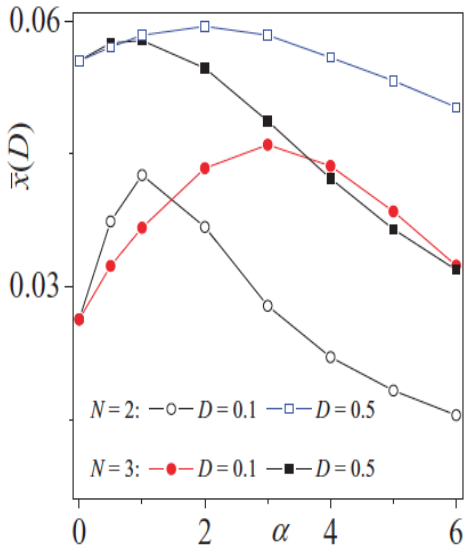

Figure 2.6: The graph of $\bar{x}(D)$ versus α for the same situation as in Figure 2.5 with fixed values of N and D, see the legend. The parameter α was the magnitude of the particle-particle interaction. $\bar{x}(D)$ peaked for the relatively small values of α and then slowly decreased for larger values of α.

accessible to individual particles shrinks. This facilitates the escape of single particles through the pore. This, in turn, explains the rising branch of the curves $\bar{x}$ versus α. As the particle coupling α increases, the particles tend to form deformable clusters and exhibit plastic flow. At very large α, the switching between cavities stops, and $\bar{x}$ decays to zero. In this description the resonant dependence of $\bar{x}$ on α is less appreciable for higher noise levels.[1, 90, 91]

In summary, in this project we demonstrated how particles suspended in a double cavity with a separating membrane can diffuse across the inter-cavity pore subject to the combined actions of thermal fluctuations and periodic drives. The inter-cavity particle flow was modulated in time at the drives' frequencies with amplitudes that could be optimised by controlling the temperature of the system. This is a geometric effect: the stochastic resonance condition depends upon the shape of the cavity and the particle-particle interactions.[1]

These results may also be of interest to those who study colloidal systems. This mechanism of stochastic resonance does not depend upon the dimensionality of the system, therefore, it may lend itself to experimental verification upon colloidal systems in three dimensional geometries. However, the mecha-

nism could be affected by other effects such as pore structure and microfluidic effects. For finite size particles like translocating molecules, the crossing time varies with the wall structure inside the pores and in the vicinity of its opening. Moreover the flow of an electrolytic suspension fluid through the inter-cavity pore could cause inhomogeneous velocity and electrical fields which could affect the driven particle drift and orientation. Nevertheless, these systems specific effects could be incorporated into a reformulated Langevin equation to allow the modelling of the system.[1]

2.2 Synchronisation of geometric stochastic resonance by a bi-harmonic drive

In Chapter One, we described a simple system demonstrating stochastic resonance namely a Brownian particle jumping between the minima of a one dimensional bistable energetic potential.[2] However, as we also pointed out there, in a variety of biological systems particles move in the constrained geometries of interstices, pores or cavities, which act as particle traps.[26, 65] A particle diffusing between two such cavities, which have smooth boundaries and are connected by a narrow pore is confined theirin by a bistable entropic potential rather than an energetic one.[20] For two and three dimensional geometries, it is possible to describe the stochastic dynamics of the system in terms of the 1D reductionist approach, described in Chapter One, with a bistable potential subject to a spatially modulated diffusion function.[4] However, the reductionist approach fails to correctly approximate the stochastic dynamics of a system with sharp confining geometries. This is the case with geometric stochastic resonance in the rectangular cavities separated by a porous membrane shown in Figure 2.7.[1, 2, 66]

As we stated in Chapter One, the finite size and shape of a particle can affect its stochastic dynamics. When an elliptical particle was simultaneously driven by a constant dc and an ac driving force through a system of stacked porous membranes, it exhibited absolute negative mobility.[117] For a sufficiently small dc drive, the time averaged net velocity of the particle across the membranes was opposite in direction to that of the mean total driving force. The elongated shape of the particle was responsible for this absolute negative mobility. Moreover, it could not have occurred for non-extensive point like particles except in the presence of channels with specially tailored walls.[2, 102, 103]

With these considerations in mind, we investigated stochastic resonance

[2]The research described here in Section 2.2 is published in; Read, M. Glavey, R. Marchesoni, F. and Savel'ev, S. (2013), 'Synchronisation of geometric stochastic resonance by a bi-harmonic drive', *European Physical Journal B*, 87, pp. 206 - 211.

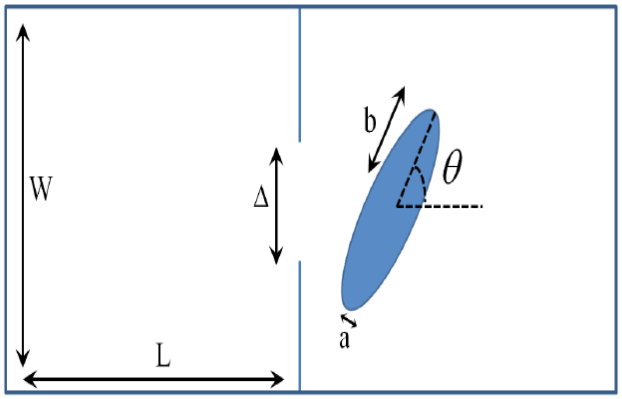

Figure 2.7: The double chamber used to demonstrate out-of-phase geometric stochastic resonance. The chamber length, width and pore width were denoted by L, W and Δ respectively. The semiminor and semimajor axes of the elliptical particle were denoted by a and b respectively.[2]

when an elliptical particle was driven across the two dimensional narrow pore of the confining geometry shown in Figure 2.7 by a bi-harmonic ac drive with one frequency much lower than the other. As we describe below, it was found that the low frequency component of the system response reached a maximum amplitude when it oscillates out of phase with the low frequency driving force component. This effect is distinct from the harmonic mixing of two commensurate frequencies through a nonlinear device investigated in both stochastic resonance and ratchet devices.[2, 69, 70, 71, 72, 73, 74] The form of stochastic resonance described here is more robust. It does not require the two driving frequencies to be commensurate and the output signal is not sensitive to the relative phase of the two harmonic components of the driving force. We also show that with increasing amplitude of the low frequency driving force, the phase lag between the system response and the driving force suddenly dropped to zero. This was taken to indicate the sharp transition from out-of-phase stochastic resonance to ordinary in-phase stochastic resonance. In addition, at larger amplitudes of the low frequency driving force, it was found that the high frequency system response underwent stochastic resonance with the opposite phase shift than in the absence of the low frequency drive.[2]

2.2.1 Model

The Brownian motion of an elliptical particle with semi-minor axis a and semi-major axis b, can be described by the position given by its centre and the orientation given by the angle θ between its semi-major axes and the pore axis, see Figure 2.7. The dynamics of this particle was simulated in two dimensions by the overdamped Langevin equations 2.16, 2.17.

$$\frac{d\vec{r}}{dt} = F(t)\vec{e}_x + \sqrt{D_r}\vec{\xi}(t). \tag{2.16}$$

$$\frac{d\theta}{dt} = \sqrt{D_\theta}\xi_\theta. \tag{2.17}$$

Here $\vec{r}(t) = (x(t), y(t))$ was the particle position at time t. $F(t)$ was the modulus of the driving force oscillating in time and directed along the pore axis. The vector $\vec{e}_x$ was the unit vector along the x axis. The fluctuating variables $\vec{\xi} = (\xi_x, \xi_y)$ and ξ_θ were independent Gaussian white noises with zero means $\langle\vec{\xi_r}\rangle = 0, \langle\xi_\theta\rangle = 0$ and delta-like autocorrelation functions, $\langle\xi_i(t), \xi_j(0)\rangle = \delta_{i,j}\delta(t)$ with $i, j = x, y$ and $\langle\xi_\theta(t), \xi_\theta(0)\rangle = \delta(t)$. The spatial and angular diffusion coefficients, D_r and D_θ were assumed to coincide $D_r = D_\theta = D$ for simplicity. Inertial and hydrodynamic effects were neglected to simplify the modelling.[2, 75, 117]

In the previous work on absolute negative mobility, which we described briefly in Section 1.5 of Chapter One, it was found that the most pronounced results were achieved for a square-wave ac drive, instead of a sinusoidal drive.[117] Consequently, a square-wave drive was used in this simulation as given by equation 2.18

$$F(t) = A_1 sign[\cos(\omega_1 t + \phi)] + A_2 sign[\cos(\omega_2 t)], \tag{2.18}$$

where A_1 and A_2 were the amplitudes of the two distinct drive components with frequencies chosen to be far apart $\omega_1 \ll \omega_2$, so as to avoid the occurrence of commensurability effects upon the resultant stochastic resonance and ϕ was their relative phase. The phase ϕ was set to zero everywhere except in the curve with open circles in Figure 2.10. The $sign(...)$ of equation 2.18 denoted the $sign$ function wherein $sign(x) = 1$ for $x > 0$, $sign(x) = -1$ for $x < 0$ and $sign(x) = 0$ for $x = 0$. Equations 2.16 and 2.17 were numerically integrated with the assumption that the system had perfectly reflecting boundary walls and elastic particle-boundary collisions.[2, 19]

In the presence of the bi-harmonic drive, the Brownian trajectories $x(t)$ of the elliptical particle embedded two persistent oscillating components resulting from the low and high frequency drives, $\bar{x}_1(D)\cos(\omega_1 t + \alpha_1(D))$ and $\bar{x}_2(D)\cos(\omega_2 t + \alpha_2(D))$, whose amplitudes, $\bar{x}_1(D)$ and $\bar{x}_2(D)$, and respective

delay phases, $\alpha_1(D)$ and $\alpha_2(D)$, can be estimated numerically by calculating

$$\bar{x}_k(D)\cos\alpha_k(D) = \frac{1}{T}\int_0^{t_{max}} x(t)\cos(\omega_k t)dt, \tag{2.19}$$

$$\bar{x}_k(D)\sin\alpha_k(D) = \frac{1}{T}\int_0^{t_{max}} x(t)\sin(\omega_k t)dt, \tag{2.20}$$

where $k = 1, 2$, were the low and high frequency drive components respectively and t_{max} was the simulation time. This asymptotic estimation of α_k held as long as the system response to both harmonic components of the drive did not mix. In the case where ω_1 and ω_2 were commensurate and insufficiently spaced, a more accurate spectral analysis would have been required.[2, 76]

When the second component of the drive was switched off, $A_2 = 0$, the system response showed standard geometric stochastic resonance, with $\bar{x_1}(D)$ passing through a maximum for an increased noise intensity D, as shown in Figure 2.8(a). The delay angle, $\alpha_1(D)$, also showed a maximum at a different value of the noise intensity. This is a typical feature of geometric stochastic resonance for point like particles in a double cavity.[1, 2] However, the optimal noise levels which maximised $\bar{x}_1(D)$ and $\alpha_1(D)$, depended upon the shape of the particle and thus provided an additional way of controlling geometric stochastic resonance. Moreover, it signified a consideration of geometric stochastic resonance to include chamber geometry and particle shape. A similar geometric stochastic resonance behaviour was displayed in Figure 2.8(b), where the system was driven only by the high frequency drive component with $A_1 = 0$.[2]

2.2.2 bi-Modal Stochastic Resonance

When both harmonic components of the drive were active, $A_1 \neq 0$ and $A_2 \neq 0$, the system response could be measured to either the forcing frequency, ω_1 or ω_2. This enabled a study of how the drive at frequency ω_2 affected the system response at frequency ω_1 and vice versa. The phenomenon of absolute negative mobility had suggested that under appropriate geometric constraints a harmonic drive could result in the drift of an elongated particle against a weak constant bias.[2, 117] In the present setup, the role of the constant bias was fulfilled by the low frequency drive component.[2]

For the system considered, an effect similar to this absolute negative mobility was observed for weak amplitudes of the low frequency driving force in equation 2.18, as shown by the red curves in Figure 2.9(a-d). In the red curve of Figure 2.9(c), the low frequency system response, $\bar{x}$, increased with the noise intensity, until it reached a maximum at $D \approx 0.04$, and then declined almost to zero. The drop in the decaying tail of the $\bar{x}_1(D)$ curve coincided with the max-

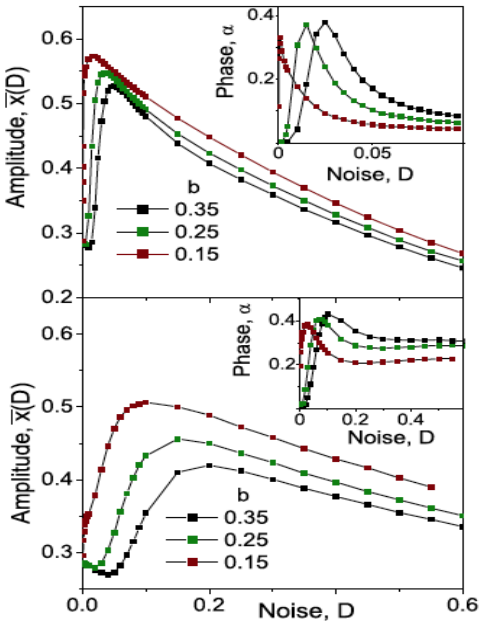

Figure 2.8: Amplitude of the system response, $\bar{x}$, versus noise level $D = D_r = D_\theta$, for a harmonic drive $F(t)$ as in equation 2.18. In the top panel (a) $A_1 = 1, A_2 = 0$, and $\omega_1/2\pi = 0.001$, and in the bottom panel (b) $A_1 = 0, A_2 = 2$, and $\omega_1/2\pi = 0.01$. The cavity geometry was such that $L = 1, W = 1 \text{and} \Delta = 0.2$. The particle semi-minor axis was $a = 0.05$ and b was as is given in the panel legends. The insets in each panel show the delay phase α versus D for the same geometry as in the main panel. The integration time used for the simulations was $dt = 1 \times 10^{-4}$, for a runtime $T = 5 \times 10^5$. [2]

imum of stochastic resonance for the $\bar{x}_2(D)$ curve. The system response delay went through a maximum at $\alpha = -\pi$ at approximately the same low D maximum of $\bar{x}_1(D)$. This occurrence was termed out-of-phase stochastic resonance. There is a connection therefore between out-of-phase stochastic resonance and absolute negative mobility, the particle crosses the pore from left to right when the low frequency drive would have driven it from right to left and the two signals get anti-synchronised for an appropriate noise level.[2]

In contrast, the system response at high frequency ω_2 was almost unaffected by the low frequency drive, see Figure 2.9 (a) and (b) red curves. The curve $\bar{x}_2(D)$ shows a standard stochastic resonance peak centred around $D = 0.2$, where out-of-phase geometric stochastic resonance was completely suppressed. The delay phase α_2, also showed resonant dependence upon D, consistent with geometric stochastic resonance with $0 < \alpha_2 < 0.5$.[1, 2, 66]

When A_1 was increased with respect to A_2, the out-of-phase stochastic resonance of the low frequency response was replaced by standard stochastic res-

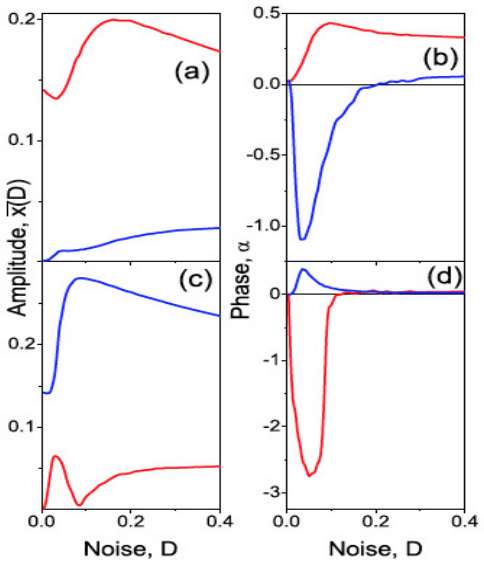

Figure 2.9: Graphs of noise dependence of system response parameters $\bar{x}_2$ (a), α_2 (b), $\bar{x}_1$ (c) and α_1 (d), on D for weak ($A_1 = 1$ red curves) and strong ($A_1 = 4$ blue curves) low frequency drive components. The drive $F(t)$, refer to equation 2.18, was such that $A_2 = 2, \omega_1/2\pi = 0.001$ and $\omega_2/2\pi = 0.01$. Out-of-phase stochastic resonance occurred for $\bar{x}_1$ at low A_1, where $\alpha_1 \simeq -\pi$ (red curve in panel (d)). Stochastic resonance for $\bar{x}_2$ at high A_1 was signalled by the dip $\alpha_2 \simeq -\pi/2$ of the blue curve in panel (b). [2]

onance with $\bar{x}_1(D)$ exhibiting a broad peak centred around $D \approx 0.1$, see Figure 2.9(c) blue curve. The phase shift, α_1, was always positive with $0 < \alpha_1 < 0.5$ and reached a maximum at $D \approx 0.5$, see Figure 2.9(d) blue curve. The affect of the drive component increased with the low frequency, ω_1, on the system response at the high frequency, ω_2. This mode interplay resulted in a small side peak on the broad curve for $\bar{x}_2(D)$, which became discernable at $D \approx 0.1$, see Figure 2.9(a) blue curve. This secondary $\bar{x}_2$ peak corresponded to a negative dip of the related phase shift with $|\alpha_2|$ never exceeding $\pi/2$. This meant that the system response at high frequency never undergoes anti-sychronisation, or out-of-phase stochastic resonance. The resonance condition, $\alpha_2 \approx -\pi/2$, could be due to the elliptical particle tending to cross the membrane pore from left to right only when the high frequency component of $F(t)$ dropped to zero and turned from negative to positive and visa versa, (or in other words the particle crosses the membrane when its drive was switched off). This is the opposite of the phase shift observed in standard stochastic resonance.[2]

Figure 2.10 shows that large delay phases α_1 were only possible upon elongating the elliptical particle so that its major axes was greater than the pore

width, $2b > \Delta$. To investigate how the particle shape affected the out-of-phase stochastic resonance of $\bar{x}_1(D)$, the Langevin equations 2.16, 2.17 were integrated for different values of the elongation aspect ratio b/a. For weak low frequency amplitudes of $F(t)$, the out-of-phase stochastic resonance was the strongest at large values of b/a. The drive phase α_1 approached $-\pi$, see Figure 2.10(d), which coincide with a large peak of $\bar{x}_1$ at low noise intensity D. As shown in Figure 2.9, the out-of-phase peak was followed by a sharp dip and slowly rising recovery branch. This dip was related to the stochastic resonance maximum of $\bar{x}_2$. As the length of the semi-major axes of the elliptical particle decreased below the pore width, $2b \leq \Delta$, out-of-phase stochastic resonance was totally suppressed. To investigate the possible dependence of this phenomenon on the relative phase of the drive component in equation 2.18, the system response for different values of ϕ were simulated. The results for $\phi = \pi/2$ are shown in Figure 2.10 with circles. They coincide with the blue curves obtained for the same simulation parameters but with $\phi = 0$. This indicates the absence of the response on the relative phase of low and high drives.[2]

The system response at high frequency, showed little sensitivity to the variation of b/a for either $\bar{x}_2(D)$ or $\alpha_2(D)$. The only noticeable change with decreasing b/a was the disappearance of the small minima of $\bar{x}_2$ at low D. This was already known to occur from Figure 2.8(b) at large b/a even in the absence of a low frequency drive.[2]

To investigate the possible effects due to the harmonic mixing of the two response components with frequencies ω_1 and ω_2 respectively, we plotted in Figure 2.11 the power spectral densities of $x(t)$ for the simulation parameters corresponding to the blue curves in Figure 2.10. The noise level was chosen so as to have one spectrum for D below the out-of-phase stochastic resonance condition (a1,a2), one spectrum at out-of-phase stochastic resonance (b1,b2), one spectrum between the out-of-phase stochastic resonance peak and the minimum response for ω_1 (c1,c2), one spectrum at the minimum of the ω_1 response (d1,d2), and one above this minimum (e1,e2). The full range spectra are shown in the left hand panels, (a1,b1,c1,d1,e1) and an enlargement of the low frequency portion in the right hand side panels (a2,b2,c2,d2,e2). Only odd harmonics of both driving frequencies were detectable and their amplitude decreased rapidly with the order number. In conclusion, Figure 2.11 indicated that (i) the generation of harmonics of either fundamental component of the process $x(t)$ could be ignored; (ii) for the values of ω_1 and ω_2 simulated, no significant mixing occurred between the low and high frequency spectra of $x(t)$, even if commensurate. This validates our spectral stochastic resonance analysis based only on the fundamental response components to drive frequency, ω_1 and ω_2.[2]

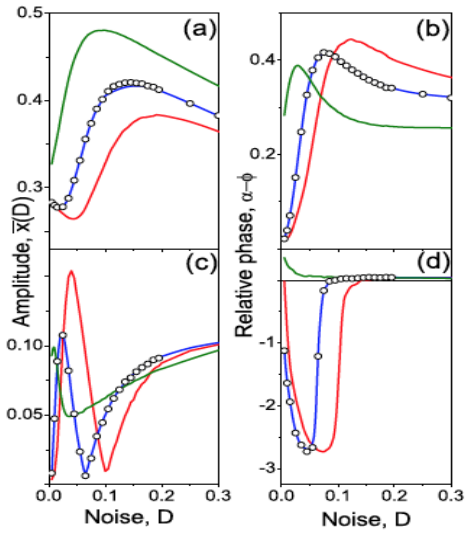

Figure 2.10: The dependence of out-of-phase stochastic resonance on the particle elongation ratio b/a, for $\bar{x}_2$ (a), α_2 (b), $\bar{x}_1$ (c) and α_1 (d), for weak low frequency drive, $\omega_1/2\pi = 0.001$ and $A_1 = 1$ and a strong high frequency drive, $\omega_2/2\pi = 0.01$ and $A_2 = 2$. The elongation aspect ratios were: $b/a = 3$, green curves, 5, blue curves and 7 red curves. The signature of out-of-phase stochastic resonance, a maximum of $\bar{x}_1(D)$ for $\alpha_1(D) \simeq -\pi$, was suppressed on decreasing b/a, as can be seen from comparing curve pairs of different colours in panels (c) and (d). No dependence on the relative drive phase ϕ was observed. For example, the open circles were obtained for the same parameters as the blue curves but with $\phi = \pi/2$ instead of $\pi = 0$.[2]

In summary, the geometric stochastic resonance of an elliptical particle in a two dimensional double cavity with a pore in the inter-cavity membrane was affected and could be controlled by the particle shape. Out-of-phase stochastic resonance for the system response at the lower frequency resulted when a bi-harmonic drive was applied parallel to the pore axis. This out of phase stochastic resonance occurs under quite general conditions namely:(i) that the lower frequency was much smaller than the higher frequency, (ii) the lower frequency drive component had a relatively lower amplitude and (iii) the elliptical particle had a high elongation aspect ratio, with the particle length $2b$ greater than the pore width Δ. The effect that particle shape had here upon geometric stochastic resonance is analogous to the effect it had previously been shown to have upon absolute negative mobility reviewed in Chapter One. Indeed, the former work partly motivated the latter. Furthermore, for strong low frequency drive components, the interplay between the two driving frequencies mostly af-

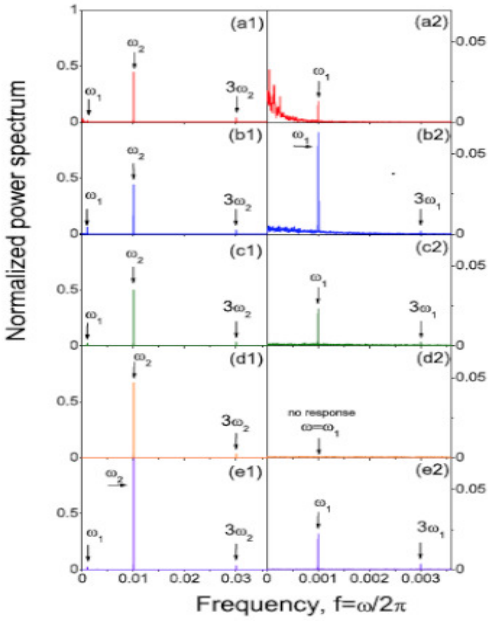

Figure 2.11: The normalised power spectrum from the $x(t)$ trajectories of Figure 2.10 for $b/a = 5$ and noise levels $D = 0.01$ (a1,a2), $D = 0.02$ (b1,b2), $D = 0.04$ (c1,c2), $D = 0.06$ (d1,d2) and $D = 0.12$ (e1,e2). The power spectra were proportional to $\langle|\hat{x}(\omega)^2|\rangle$, with $\hat{x}(\omega)$ denoting the Fast Fourier Transform of $x(t)$, and normalised to the spectrum peak at $\omega = \omega_2$ in panel (e1). The panels on the left (a1,b1,c1,d1,e1) represent the spectra over the entire ω domain while panels on the right (a2,b2,c2,d2,e2) show the spectral details around the low drive frequency ω_1.[2]

fected the high frequency system response by inverting the optimal stochastic resonance phase shift from $\pi/2$ to $-\pi/2$. Both effects were relatively insensitive to the choice of the frequencies, the relative phase or waveform for the two drives. This indicated that the robust nature of the phenomenon. Experimental verification of this out-of-phase stochastic resonance could be demonstrated in a mixture of charged rodlike colloidal particles driven on a disordered substrate by a bi-harmonic electric field.[2] This project represented a logical advance upon earlier work upon geometric stochastic resonance wherein the research focused on chamber and pore geometry.[2, 115, 117] In our later work, described in Chapter Three, we have demonstrated how not only particle geometry but its variation in time also affects stochastic dynamics.

Chapter 3

Rectification

In Chapter Three we describe our research related to the rectification of Brownian particles with oscillating radii freely diffusing in an asymmetric corrugated channel. The stochastic transport was simulated over a range of driving forces for a series of temperatures and angular frequencies of radial oscillation. Here we show that there was a strong influence of self-oscillation frequency upon the average particle velocity. This effect can be used to control the rectification of biologically active particles as well as their separation according to their activity. For instance, it can be used in the separation of living and dead cells.[3]

3.1 Rectification of Brownian Particles with Oscillating Radii in Asymmetric Corrugated Channels

Rectification is the process of turning the unbiased fluctuations, or oscillating drives with zero average, in a system into the directed transport of particles. One means by which this is accomplished is by the use of ratchets. As we said in Chapter One, a ratchet is a device that is capable of transporting particles in a periodic structure with non-zero macroscopic velocity, although on average no macroscopic force is acting. This is achieved through the breaking of temporal and/or spatial symmetry.[3, 94, 95, 96, 97]

Interest in rectification partly stems from its potential application on the nano-scale where Brownian motion predominates, yet it can deliver directed transport of biological probes and nano-devices, as well as, facilitate particle separation technologies. However for practical implementation to be achieved, it is apparent that chamber and particle geometry must be considered.[3]

With respect to chamber geometry, it is known that in a many biological sys-

tems particles move in confined geometries, such as cavities and channels which act as traps or guide particle motion. When particles diffusing between such cavities are surrounded by smooth channels connected by narrow pores they are confined in each cavity by an entropic rather than an energetic potential.[1, 66] In these cases a Fokker-Plank or Langevin equation can be used to model the diffusion dynamics of these particles in two and three dimensions. Then at low values of the driving force, approximate solutions can then be obtained by reducing the problem to Brownian diffusion in an effective 1D periodic potential using a Fick-Jacobs kinetic equation with a spatially dependent diffusion function and a 1D entropic barrier replacing the geometric constraints. However, at higher values of the driving force, the average particle current and the effective diffusion diverge from the values obtained by the 1D reductionist approach. It is to be remembered that this occurs because the assumption of a transversely uniform density distribution introduced in the Fick-Jacobs approximation to eliminate transverse coordinates, is no longer valid at strong driving forces. Examples of when the 1D reductionist approach has proved inadequate include geometric stochastic resonance (gSR) in a double cavity and Brownian motion in septate channels.[1, 2, 66, 84] There are limits therefore to the applicability of the 1D reductionist approach, as we have related in Chapter One. For sharper boundaries and or larger driving forces, we must directly integrate the 2D Langevin equation by using, for example the Euler method, as we have done here.[1, 2, 19, 20, 26, 66, 98, 99]

As we mentioned in Chapter One, interest in particle shape and its effect upon stochastic dynamics is increasing in part due to the potential applications of Janus particles.[3, 39] Researchers are investigating the additional functionality that can be conferred upon Janus particles by making them active particles, such as self oscillating or self-propelled particles.[39, 44] Methods of propulsion might be found at the mesoscopic level where bacteria use various modes of self-propulsion including: flagellar motion, gliding motility, tumbling, screwing and twitching.[33, 34, 35] But whatever means of self-propulsion emerges at the nano level, it must contend with the challenge of Brownian motion and the need for a non-equilibrium source of energy to achieve directed motion.[33] With these considerations in mind, we modelled Janus-like particles in a geometric ratchet composed of an asymmetric corrugated channel, wherein the particles have an element of self-propulsion by means of oscillating radii.[3]

3.2 Model

In our model we considered an overdamped Brownian circular particle with an oscillating radius freely diffusing in a 2D suspension fluid confined in an

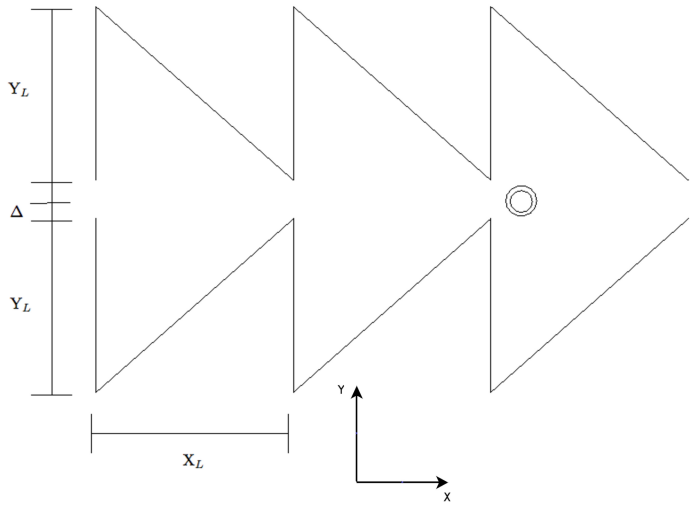

Figure 3.1: Brownian particle with oscillating radius freely diffusing in a 2D asymmetric corrugated channel with reflecting boundaries. The sharp confining geometry is such that the 1D reductionist approach cannot correctly approximate the stochastic dynamics and a 2D Langevin model is required. The concentric circles represent the lower and upper limits of the particle's oscillating radius, $R = R_1 + R_2 = a + b|\cos \omega t|$. Chamber parameters were: $X_L = Y_L = 1$, $\Delta = 0.1$.[3]

asymmetric corrugated channel with reflecting walls as shown in Figure 3.1. The overdamped dynamics of the particles were modelled by the Langevin equation:[6, 106]

$$\frac{d\vec{r}}{dt} = -A(t)\vec{e}_x + \sqrt{D}\vec{\xi}(t), \tag{3.1}$$

where $\vec{r}$ was the position vector of the particle, $A(t)\vec{e}_x$ was the driving force along the x axis, $\vec{e}_x$ was the unit vector along the x axis, D was the noise intensity and $\vec{\xi}(t) = [\xi_x(t), \xi_y(t)]$ was the zero mean Gaussian white noise with autocorrelation function $\langle \xi_i(t)\xi_j(t')\rangle = 2\delta_{ij}\delta(t - t')$ with $i, j = x, y$. We used a driving force $A(t) = F\,\mathrm{sign}(\cos(\pi t/t_{\max}))$ with simulation time $t_{\max}$ and $\mathrm{sign}(z) = 1$ for $z > 0$ and $\mathrm{sign}(z) = -1$ for $z < 0$. Thus the ac force $A(t)$ pushed the system to the left during the first half time of simulation and to the right during the second half time of simulation resulting in no average dc drive. Therefore, the average velocities reported in Figures 3.2 and **??** below originated from the rectification mechanism. The particle had a fixed internal component of radius $R_1 = a$ and an oscillating external component of radius $R_2 = b|\cos \omega t|$, that is $R = R_1 + R_2 = a + b|\cos \omega t|$, where a and b were constants and $max|R_2| < R_1$. Equation 3.1 was numerically integrated using a Euler algorithm. The number of time steps used was 10^9 (time step was 10^{-4} and simulation time was 10^5).[3, 106, 107]

3.3 Rectification and Biologically Active Particles with Oscillating Radii

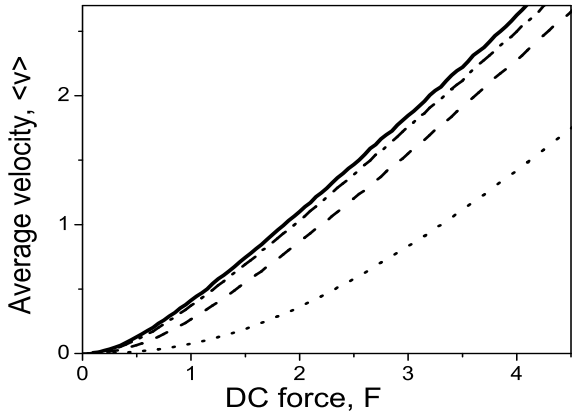

Figure 3.2: Average velocity of a single circular particle of constant radius, $R(t) = R_1$ and $(R_2 = 0)$ as a function of driving force F for several values of $R_1/\Delta = 0.5$ (solid), 0.8 (dash-dot), 0.95 (dash-dash), 0.99 (dot-dot) with pore half-width $\Delta = 0.1$, and $D = 0.1$, see also Figure 3.1.[3]

Figure 3.2 shows rectification of the single circular particle of constant radius $(R(t) = R_1, R_2 = 0)$ for several temperatures and a wide range of DC driving forces. At low driving forces, the rectified velocity increased as F^2 and then linearly increased. This behaviour is quite different from the usual rectification peak in 1D.[3]

Figure **??** shows rectification of a self-oscillating particle with a radius composed of a fixed internal component of radius $(R_1 = 0.09)$ and an oscillating external component of radius $(R_2 = 0.03|\cos\omega(t)|)$ for fixed temperature $D = 0.1$ and a range of angular speeds of oscillation. Thus the particle had a minimum radius of (0.09) and a maximum of (0.12), in a corrugated channel where the pore half-width was $\Delta = 0.10$. This led to a gating mechanism whereby maximal rectification could be achieved when there existed an average time t_e which the particle needed to pass a channel cell (note that this time was controlled by driving amplitude F and noise) and the particle's period of oscillation t_o, where $t_o = 2\pi/\omega$: that is when $t_e \approx nt_o$ and $(n = 1, 2, 3...)$. The oscillation in each curve for ω occured because with increased driving force the value of t_e fell successively in and out of commensurability with t_o leading to varying amplitude of rectification. When $t_o \approx t_e$ the particle as 'seen" by successive pores most closely resembled a particle of constant radius and thus its rectification most closely resembled that of a particle of constant radius too. The time needed for

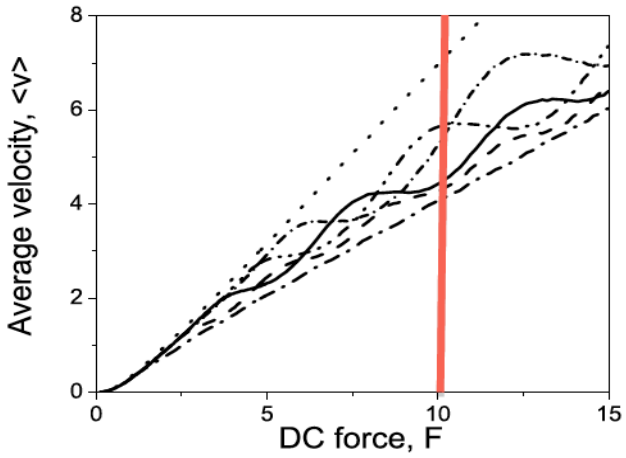

Figure 3.3: Average velocity of a self-oscillating particle with an oscillating radius ($R_1 = 0.9\Delta$, $max|R_2| = 0.3\Delta$), diffusion constant $D = 0.1$ and a range of oscillation frequencies. As can be seen from the red line, for a given value of the driving force ($F = 10$), particles have different average velocities according to their angular frequency of oscillation and can thus be separated.[3]

the particle to traverse the chamber was estimated as $\Delta T = X_L/V = X_L/F$ where V is the velocity of the particle and F is the amplitude of the driving force. To pass through to the next chamber, the particle should have the minimum size, which occurs at $T_n = n\pi/\omega$ where $(n = 1, 2, 3...)$, the optimal force can be estimated as $F_n = X_L\omega/n\pi$. It is apparent therefore that differential rectification of populations of Brownian particles freely diffusing in asymmetric corrugated channels can be controlled by means of differing angular frequencies of oscillations and used to achieve particle separation. This will be of interest to those seeking to achieve controllable and directed transport of self-oscillating particles on the nano-scale such as that of self-propelled Janus particles. Moreover, it could also be used for the separation of living and dead cells.[3]

We have demonstrated rectification for a self-ocillating Brownian particle in a series of asymmetric corrugated channels. Rectification could be optimised for frequency ω of radial oscillation by matching the mean noise and driving force induced escape time t_e with the period of oscillation t_o. This mechanism can be used for separation of self-oscillating particles according to their self-frequencies (for instance living and dead cells or bacteria) on the nano-scale. This rectifi-

cation behaviour cannot be obtained by the 1D reductionist approach.[3]

Chapter 4

Conclusions and Outlook

In the concluding chapter of my thesis, we summarise our research findings, draw out the research themes and offer some concluding remarks on the impact of this work upon the progress of this research area.

In Chapter One, we defined and described in turn stochastic dynamics, stochastic resonance, geometric stochastic resonance, rectification and absolute negative mobility. We considered the modelling of stochastic dynamics in one and higher dimensions and the limitations of the 1D reductionist approach. We concluded with a consideration of some of the applications of stochastic transport.

In the first part of Chapter Two, we demonstrated how particles suspended in a double cavity with a separating membrane could diffuse across the inter-cavity pore subject to the combined actions of thermal fluctuations and periodic drives. The inter-cavity flow was modulated in time at the drives' frequencies with amplitudes that could be optimised by controlling the temperature of the system. This is a geometric effect, where the stochastic resonance condition depends upon the shape of the cavity and the particle-particle interactions.[1]

These results may be of interest in the study of colloidal systems. The mechanism of stochastic resonance described does not depend upon the dimensionality of the system, therefore, it may lend itself to experimental verification upon colloidal systems in three dimensional geometries. However, this form of stochastic resonance could be affected by other competing effects such as pore structure and microfluidic effects. For translocating molecules in nanoscale systems, the transit time varies with the internal structure of the pore and the structure in the vicinity of its opening. For an electrolytic suspension fluid flowing across an inter-cavity pore, inhomogeneous velocity and electrical fields can affect the drift and orientation of the driven particles. However, these systems specific effects can in be assimilated into the Langevin model using an appropriate potential

term.[1]

In the second part of Chapter Two, we demonstrated that geometric stochastic resonance in a two dimensional double cavity with a pore in the inter-cavity membrane was affected and could be controlled by particle shape. Out-of-phase stochastic resonance for the system response at the lower frequency resulted when a bi-harmonic drive was applied parallel to the pore axis. Onset occurs under quite general conditions namely: (i) that the lower frequency is much smaller than the higher frequency, (ii) the lower frequency drive component has a relatively lower amplitude and (iii) the elliptical particle has a high elongation aspect ratio, with the particle length $2b$ greater than the pore width Δ. The effect that particle shape had upon geometric stochastic resonance is analogous to the effect it had previously been shown to have upon absolute negative mobility. Furthermore, for strong low frequency drive components, the interplay between the two driving frequencies mostly affected the high frequency system response by inverting the optimal stochastic resonance phase shift from $\pi/2$ to $-\pi/2$. Both effects are relatively insensitive to the choice of frequencies, relative phase or waveform for the two drives. This indicates that they are quite robust phenomena. This work represents a logical advance upon earlier work on geometric stochastic resonance wherein the research focused on chamber and pore geometry. Moreover, it expands the spectrum of parameters that lend controllability to stochastic resonance to include particle size.[2, 117, 115]

In Chapter Three we demonstrated rectification for a self-oscillating Brownian particle in a series of asymmetric corrugated channels. Rectification could be optimised for frequency ω of radial oscillations by matching the mean noise and driving force induced escape time t_e with the period of oscillation t_o. This mechanism can be used for separation of self-oscillating particles according to their self-frequencies on the nanoscale, for instance, for the separation of living and dead cells or bacteria. This rectification behaviour cannot be obtained using the 1D reductionist approach of the Fick-Jacobs formalism but requires integration of the 2D Langevin equation.[3]

Experimental verification of our results is also possible: ion beam lithography has enabled the etching of almost any shape of confining geometry upon the surface of a type II superconductor. Moreover, effective vortex size can be indirectly controlled through temperature variation with time $T = T(t)$, $\lambda = \lambda_0/\sqrt{1 - T/T_c}$. This allows the realisation of effective radial oscillations. Hence control can be exerted over vortex dynamics through the manipulation of chamber geometry and vortex size. Our findings upon geometric stochastic resonance and rectification offer enhanced control of the stochastic dynamics of vortices in type II superconductors enabling them to be shunted away from sites of sensitive superconducting electronic devices such as SQUID magnetometers.

This enables SQUID based technologies such as MRIs to reach an enhanced level of sensitivity opening up additional diagnostic applications. Moreover stable SQUIDs have been considered as the basis for quantum computing systems.

Throughout this thesis we have attempted to draw out the research themes that motivated and informed this work. Here we offer some concluding remarks.

We were at pains in the first chapter to draw the superficially disparate topics of geometric stochastic resonance and rectification together through their common characteristic of noise. Noise is integral to these and indeed all forms of stochastic transport. Moreover, noise is the inescapable reality of the physical world at the nanoscale. Stochastic resonance has enabled us to achieve a paradigm shift in how we think of noise: where formerly we may have thought of it as a nuisance within a system, we now see it has a constructive role to play in achieving directed transport on the nanoscale or the uptake of weak coherent inputs. What evolution has been taking advantage of for millions of years in biological systems, we are only beginning to take advantage of ourselves in our design of systems on the nanoscale.

Our work has contributed to an expansion in research emphasis from a consideration of chamber geometries to particle geometries in the control of stochastic transport. This is a logical and practical extension of the ongoing research. Until recently research focused on the impact of chamber geometry on stochastic dynamics but the extensive nature of the particles themselves was not attended to. However, as our research has shown with respect to geometric stochastic resonance and rectification, and as earlier research has shown with respect to absolute negative mobility, when particle size and shape is no longer negligible with respect to chamber dimensions its geometry must be considered for its impact upon stochastic transport mechanisms. The extensive nature of the particle and its geometry adds to the controllability of stochastic transport. Moreover, it is not always possible to control chamber geometry, such as in drug delivery systems, but it is possible to exercise some control over particle geometry. The promising applications of Janus particles and active particles, e.g. with oscillating size, their extensive nature and asymmetric design ensure a continued requirement to understand and control the impact of particle geometry upon stochastic transport. Thus it is envisaged that research upon the impact of particle geometry on stochastic transport will continue apace.

We have also attempted to draw the reader's attention to the inadequacy of the 1D reductionist approach in accurately modelling sharp confining geometries or the stochastic dynamics of extensive particles. Geometric stochastic resonance and the rectification of extensive particles demands an alternative approach, such as integration of the 2D Langevin equation, to fully realise the complex dynamics, as demonstrated by the models and results of Chapters Two

and Three.

It is also worthwhile remarking once more upon the pervasive nature of stochastic resonance from the earth's glaciation cycle, to neurosensory systems, to vortex dynamics and nanotechnology, it continues to provide us with a very interesting journey.

We should also acknowledge in passing the power of simple mathematical modelling of the Langevin equation to tackling problems in areas as apparently diverse as those of fluxonics and particle transport in biophysics.

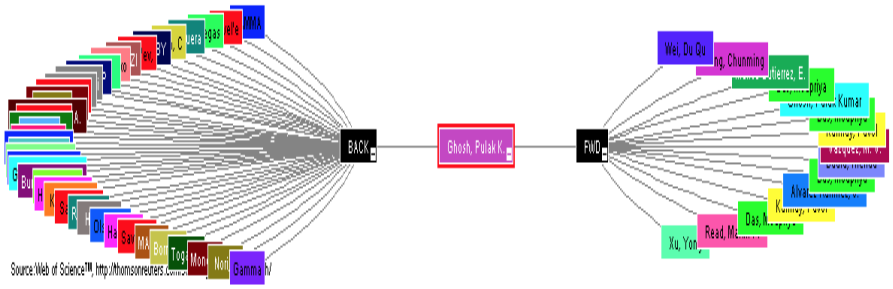

Figure 4.1: The figure shows a 'citation map' for our first paper 'Geometric stochastic resonance in a double cavity'.[1] The central rectangle represents our paper. The coloured rectangles to the left represent the individual papers we have referenced in our work, while the coloured rectangles to the right represent the papers that have referenced our work since its publication in 2011. For instance, the uppermost (purple) rectangle on the right represents: Wei, D.Q. Mai, X.H. Chen, H.B. Luo, X.S. Zhang, B. Zeng, S.Y. Tang, G.N. (2014), 'Transport properties of inertial particles in networks with random long-range interactions', *Physica A Statistical Mechanics and its applications*, 394, pp. 358 - 364.[118]

As a crude but succinct metric of the impact of our current work we include Figure 4.1. In one succinct image this shows how we have drawn on the work of others and how now others draw on this work of ours. This is the web of knowledge which we weave and we are happy to have woven a strand or two.

Finally, it is expected that research upon the use and control of stochastic dynamics on the nanoscale will continue to be of increasing importance in the

years to come in tandem with the nanosystems it attempts to model. This augurs well for the continuing relevance and impact of our research as well as the need for its advancement.

Appendix A

Programs and Datasets

The programs and datasets associated with the individual projects that compose this thesis are available upon request.

Appendix B

Bibliography

Bibliography

[1] Ghosh, P.K. Glavey, R. Marchesoni, F. Savel'ev, S.E. Nori, F. (2011) 'Geometric stochastic resonance in a double cavity', *Physical Review E*, 84, 011109.

[2] Read, M. Glavey, R. Marchesoni, F. and Savel'ev, S. (2013), 'Synchronisation of geometric stochastic resonance by a bi-harmonic drive', *European Physical Journal B*, 87, pp. 206-211.

[3] Glavey, R. and Savel'ev, S. (2015), 'Rectification of Brownian particles with oscillating radii in asymmetric corrugated channels', *Acta Physica Polonica*, submitted Aug 2014 - awaiting publication.

[4] Burada, P.S. Hänggi, P. Marchesoni, F. Schmid, G. and Talkner, P. (2009), 'Diffusion in Confined Geometries', *ChemPhysChem*, 10, pp. 45 - 54.

[5] Giancoli, D.C. (2009), *Physics for scientists and engineers with modern physics*, 4th edn, New Jersey: Prentice Hall.

[6] Lemons, D.S. Gythiel, A. (1997), 'Paul Langevin's 1908 paper "On the theory of Btownian motion"', *(*American Journal of Physics, 65, (11), pp. 1079 - 1081.

[7] Wei, Q-H. Bechinger, C. and Leiderer, P. (2000), 'Single-file diffusion of colloids in confined channels', *Science*, 287, 5453, pp. 625-627, 101126.

[8] Cui, B. Diamant, H. and Lin, B. (2002), 'Screened hydrodynamic interaction in a narrow channel', *Physical Review Letters*, 89, 188302.

[9] Zwanzig, R. (1992), 'Diffusion past an entropic barrier', *Journal of Physical Chemistry*, 96, 10, pp. 3926 - 3930, 101021.

[10] Reguera, D. and Rubi, J.M. (2001), 'Kinectic equations for diffusion in the presence of entropic barriers', *Physical Review E*, 64, 061106.

[11] Kalinay, P. and Percus, J.K. (2006), 'Corrections to the Fick-Jacobs equation', *Physical Review E*, 74, 041203.

[12] Burada, P.S. Schmid, G. Reguera, D. Rubi, J.M. and Hänggi, P. (2007), 'Biased diffusion in confined media: Test of the Fick-Jacobs approximation and validity criteria', *Physical Review E*, 75, 051111.

[13] Reguera, D. Schmid, G. Burada, P.S. Rubi, J.M. Reimann, P. and Hänggi, P. (2006), 'Entropic transport: Kinetics, scaling and control mechanisms', *Physical Review Letters*, 96, 130603.

[14] McDonnell, M.D. Abbot, D. 2009, 'What is stochastic resonance? Definitions, misconceptions, debates, and its relevance to biology', *PLoS Computational Biology*, 5, 5, pp. 1 - 8, e1000248.

[15] Hänggi, P. Talkner, P. and Borkovec, M. (1990), 'Reaction-rate theory: fifty years after Kramers', *Review of Modern Physics*, 62, pp. 251 - 342.

[16] Reimann, P. Van den Broeck, C. Linke, H. Hänggi, P, Rubi, J.M. Perez-Madrid, A. (2001), 'Giant acceleration of free diffusion by use of tilted periodic potentials', *Physical Review Letters*, 87, 010602.

[17] Reimann, P. Van den Broeck, C. Linke, H. Hänggi, P. Rubi, J.M. and Perez-Madrid, A. ,(2002), 'Diffusion in tilted periodic potentials: Enhancement, universality and scaling', *Physical Review E*, 65, 031104.

[18] Burada, P.S. Schmid, G. Talkner, P. Hänggi, P. Reguera, D. Rubi, J.M. (2008), 'Entropic particle transport in periodic channels', *Biosystems*, 93, 1 - 2, pp. 16 - 22, 101016.

[19] Marchesoni, F. and Savel'ev, S. (2009), 'Rectification currents in two-dimensional artificial channels', *Physical Review E*, 80, 011120.

[20] Burada, P.S. Schmid, G. Reguera, D. Vainstein, M.H. Rubi, J.M. and Hänggi, P. (2008), 'Entropic stochastic resonance', *Physical Review Letters*, 101, 130602.

[21] Laach, N. Kenward, M. Yariv, E. and Dorfman, D. (2007), 'Force-driven transport through periodic entropy channels', *EPL*, 20, 5, 101209.

[22] Ai, B-Q. and Liu, L-G. (2006), 'Current in a three-dimensional periodic tube with unbiased forces', *Physical Review E*, 74, 051114.

[23] Reimann, P. (2002), 'Brownian motors: noisy transport far from equilibrium', *Physical Reports*, 361, pp. 57 - 265.

[24] The Editors of Encyclopdia Britannica, (2014), available at: http://www.britannica.com/EBchecked/topic/125898/colloid, (accessed 14th December 2014).

[25] Ma, X-G, Lai, P-Y and Tong, P. (2013), 'Colloidal diffusion over a periodic energy landscape', *Soft Matter*, 9, pp. 8826 - 8836.

[26] Hänggi, P. Marchesoni, F. (2008), 'Artificial Brownian motors: Controlling transport on the nanoscale', *Reviews of Modern Physics*, 81, 1, pp. 387 - 442.

[27] Crocker, J.C. and Grier, D.G. (1996), 'Methods of digital video microscopy for colloidal studies', *Journal of Colloid and Interface Science*, 179, 1, pp. 298 - 310.

[28] Reimann, P. Van den Broeck, C. Linke, H. Hänggi, P. Rubi, J.M. and Pérez-Madrid, A. (2001), 'Giant acceleration of free diffusion by use of tilted periodic potentials', *Physical Review Letters*, 87, 010602.

[29] Lee, S-H, Grier, D.G. (2006), 'Giant colloidal diffusivity on corrugated optical vortices', *Physical Review Letters*, 96, 190601.

[30] Korda, P.T. Taylor, M.B. and Grier, D.G. (2002), 'Kinetically locked in colloidal transport in an array of optical tweezers', *Physical Review Letters*, 89, 12, 128301.

[31] Ma, X-G, Lai, P-Y, Ackerson B.J. and Tong, P. (2014), 'Colloidal transport and diffusion over a tilted periodic potential: dynamics of individual particles', *Soft Matter*, pp. 1 - 16.

[32] Rousselet, J. Salome, L. Adjari, A. and Prost, J. (1994), 'Directional motion of Brownian particles induced by a periodic asymmetric potential'. *Nature*, 370, pp. 446 - 448.

[33] Astumian, R.D. and Hänggi, P. 'Brownian motors', *Physics Today*, Nov 2002, pp. 33 - 39.

[34] McBride, M.J. (2001), 'Bacterial gliding motility: multiple mechanisms for cell movement over surfaces,' *Annual Review of Microbiology* 55, pp. 49 - 75.

[35] Merz, A.J. So, M. and Sheetz, M.P. (2000),'Pilus retraction powers bacterial twitching motility', *Nature*, 407, pp. 98 - 102.

[36] Zusman, D.R. Scott, A.E. Yang, A. and Kirby, J.R. (2007), 'Chemosensory pathways, motility and development in Myxococcus xanthus', *Nature Reviews Microbiology*, 5, pp. 862 - 872. DOI: 10.1038/nrmicro1770.

[37] Berg, H.C. 'Motile behaviour of bacteria', *Physics Today*, Jan 2002, pp. 24 - 29.

[38] Purcell, E.M. (1977), 'Life at low Reynolds number', *American Journal of Physics*, 45, pp. 3 - 11.

[39] Walther, A. and Muller, A.H.E. (2013), 'Janus particles: synthesis, self-assembly, physical properties and applications', *Chemical Reviews*, 113, pp. 5194 - 5261.

[40] Choi, J. Zhao, Y. Zhang, D. Chien, S. and Lo, Y.H. (2003) 'Patterned flourescent particles as nano probes for the investigation of molecular interactions', *Nano Letters*, 3, 8, pp. 995 - 1000.

[41] Anker, J.N. and Kopelman, R. (2003), 'Magnetically modulated optical nano probes', *Applied Physics Letters*, 82, 7, pp. 1102 - 1104.

[42] Behrend, C.J. Anker, J.N. McNaughton, B.H. Brasuel, M. Philbert, M.A. and Kopelman, R. (2004), 'Metal-capped Brownian and magnetically modulated optical nano probes (MOONs): micro mechanics in chemical and biological micro environments', *Journal of Physical Chemistry B*, 108, pp. 10408 - 10414.

[43] Synytska, A. Khanum, R., Ionov, l. Cherif, C. and Bellman, C. (2011), 'Water-repellent textiles via decorating fibers with amphiphilic janus particles', *Applied Materials and Interfaces*, 3, pp. 1216 - 1220.

[44] Gosh, P.K. Misko, V.R. Marchesoni, F. and Nori, F. (2013), 'Self-propelled Janus particles in a ratchet: numerical simulations', *Physical Review Letters*, 110, 268301.

[45] Ebbens, S.J. Howse, J.R. (2010), 'In pursuit of propulsion at the nanoscale', *Soft Matter*, 6, pp. 726 - 738.

[46] Lee, T-C. Alárcon-Corres, M. Miksch, C. Hahn, K. Gibbs, J.G. and Fischer, P. (2014), 'Self-propelling nano-particles in the presence of strong Brownian forces', *Nano Letters*, 14, 5, pp. 2407 - 2412.

[47] Howes, J.R. Jones, R.A.L. Ryan, A.J. Gough, T. Vafababakhsh, R. and Golestanian, R. (2007), 'Self-motile colloidal particles: from directed propulsion to random walk', *Physical Review Letters*, 99, 048102.

[48] Baraban, L. Makarov, D. Streubel, R. Mónch, I. Grimm, D. Sanchez, S. and Schmidt, G. (2012), 'Catalytic janus motors on microfluidic chip: deterministic motion for targeted cargo delivery', *ACS Nano*, 6, 4, pp. 3383 - 3389.

[49] Pavlick, R.A. Sengupta, S. McFadden, T. Zhang, H. and Sen, A. (2011), 'Polymerization-powered motor', *Angewandte Chemie International Edition*, 50, pp. 9374 - 9377.

[50] Savel'ev, S. (2011), Superconductivity and nanoscience, Lecture slide.

[51] Harada, K. Kamimura, O. Kasai, H. Matsuda, T. Tonomura, A. and Moshchalkov, V.V. (1996), 'Direct observation of vortex dynamics in superconducting films with regular arrays of defects', *Science*, 274, 5290, pp. 1167 - 1170.

[52] Reichhardt, C. Olson, C.J. and Nori, F. (1998), 'Commensurate and incommensurate vortex states in superconductors with periodic pinning arrays', *Physical Review B*, 57, pp. 7937 - 7943.

[53] Lee, C.-S. Jankó, B. Derényi. I. and Barabá, A.-L. (1999), 'Reducing vortex density in superconductors using the ratchet effect', *Nature*, 400, pp. 337 - 340.

[54] Costantini, G. Marchesoni, F. and Borromeo, M. (2002), 'String ratchets ac driven asymmetric kinks', *Physical Review E*, 65, 051103.

[55] Marchesoni. F. (1996), Thermal ratchets in 1+1 dimensions', *Physical Review Letters*, 77, pp. 2365 - 2367.

[56] Crisen, A. Pross, A. Cole, D. Bending, S.J. Wördendweber, Lahl, P. and Brandt, E.H. (2005), 'Anisotropic vortex channeling in $YBa_2Cu_3O_{7-\delta}$ thin films with ordered antidot arrays', *Physical Review B*, 71, 144504.

[57] Menghini, M. Van de Vondel, J. Gheorghe, D.G. Wijngaarden, R.J. and Moshchalkov, V.V. (2007), 'Asymmetry reversal of thermomagnetic avalanches in Pb films with a ratchet pinning potential', *Physical Review B*, 75, 184515.

[58] Van Look, L. Zhu, B.Y. Jonckheere, R. Zhao, B.R. Zhao, Z.X. and Moshchalkov, V.V. (2002), 'Anisotropic vortex pinning in superconductors with a square array of rectangular sub micron holes', *Physical Review B*, 66, 214511.

[59] Van de Vondel, J. de Souza Silva, C.C. Zhu, B.Y. Morelle, M. and Moshchalkov,V.V. (2005), 'Vortex-rectification effects in films with periodic asymmetric pinning'. *Physical Review Letters*, 94, 057003.

[60] Ooi, S. Savel'ev, S. Gaifullin, M.B. Mochiku, T. Hirata, K. and Nori. F. (2007), 'Nonlinear nanodevices using magnetic flux quanta', *Physical Review Letters*, 99, 207003.

[61] Gonzalez, E.M. Nunez, N.O. Anguita, J.V. Vincent, J.L. (2007), 'Transverse rectification in superconducting thin films with arrays of asymmetric defects'. *Applied Physics Letters*, 91, 062505.

[62] Villegas, J.E. Savel'ev, S. Nori, F. Gonzalez, E.M. Anguita, J.V. Garcia, R. Vicent, J.L. (2003), 'A superconducting reversible rectifier that controls the motion of magnetic flux quanta', *Science*, 302, 5648, pp. 1186 - 1191.

[63] Savel'ev, S. Misko, V. Marchesoni, F. and Nori. F. (2005), 'Separating particles according to their physical properties: transverse drift of underdamped and overdamped interacting particles diffusing through two-dimensional ratchets', *Physical Review B*, 71, 214303.

[64] Savel'ev, S. and Nori, F. (2002), 'Experimentally realisable devices for controlling the motion of magnetic flux quanta in anisotropic superconductors', *Nature Materials*, 1, pp. 179 - 184.

[65] Hänggi, P. (2002), 'Stochastic resonance in biology'. *ChemPhysChem*, 3, pp. 285 - 290.

[66] Ghosh, P.K. Marchesoni, F. Savel'ev, S.E. and Nori, F. (2010), 'Geometric Stochastic Resonance', *Physical Review Letters*, 104, 020601.

[67] Hänggi, P. Marchesoni, F. Savel'ev, S.E. and Schmid, G. (2010), 'Asymmetry in shape causing absolute negative mobility', *Physical Review E*, 82, 041121.

[68] Eichhorn, R. Reimann, P. and Hänggi, P. (2002), 'Brownian motion exhibiting absolute negative mobility', *Physical Review Letters*, 88, 190601.

[69] Gammaitoni, L. Löcher, M. Bulsara, A. Hänggi, P. Neff, J. Wiesenfeld, K. Ditto, W. and Inchiosa, M.E. (1999), 'Controlling Stochastic Resonance', *Physical Review Letters*, 82, 4574.

[70] Schmid, G. and Hänggi, P. (2005), 'Controlling nonlinear stochastic resonance by harmonic mixing', *Physica A*, 351, 1, pp. 95 - 105.

[71] Savel'ev, S. Marchesoni, F. Hänggi, P. and Nori, F. (2004), 'Transport via nonlinear signal mixing in ratchet devices', *Physical Review E*, 70, 066109.

[72] Savel'ev, S. Marchesoni, F. Hänggi, P. and Nori, F. (2004), 'Nonlinear signal mixing in a ratchet device', *Europhysics letters*, 67, 179.

[73] Savel'ev, S. Marchesoni, F. Hänggi, P. and Nori, F. (2004), 'Signal mixing in a ratchet device: commensurability and current control', *European Physical Journal B*, 40, pp. 403 - 408.

[74] Ooi, S. Savel'ev, S. Gaifullin, M.B. Mochiku, T. Hirata, K. and Nori, F. (2007), 'Nonlinear nanodevices using magnetic flux quanta', *Physical Review Letters*, 99, 207003.

[75] Manghi, M. Schlagberger, X. Kim, Y.-B. and Netz, R.R. (2006), 'Hydrodynamic effects in driven soft matter', 2, pp. 653 - 668.

[76] Jung, P. and Hänggi, (1993), 'Hopping and phase shifts in noisy periodically driven bistable systems', *Zeitschrift für Physik B*, 90, pp. 255 - 260.

[77] Gammaitoni, L. Hänggi, P. Jung, P. and Marchesoni, F. (1998), 'Stochastic Resonance', *Reviews of Modern Physics*, 70, pp. 223 - 287.

[78] Gammaitoni, L. Hänggi, P. Jung, P. and Marchesoni, F. (2009), 'Stochastic resonance: A remarkable idea that changed our perception of noise', *European Physical Journal B*, 69, 1, pp. 1 - 3.

[79] Zwanzig, R. (1992), 'Diffusion past an entropy barrier', *The Journal of Physical Chemistry*, 96, 10, pp. 3926 - 3930.

[80] Reguera, D. and Rubi, J.M. 'Kinetic equations for diffusion in the presence of entropic barriers', *Physical Review E*, 64, 061106.

[81] Hänggi, P. and Marchesoni, F. (2005), 'Brownian motors', *Annalen der Physik*, 1 - 3, pp. 51 - 70, 10.1002.

[82] Makhnovskii, Y.A. Berezhkovskii, A.M. and Zitserman, V.Y. (2009), 'Time-dependent diffusion in tubes with periodic partitions', *The Journal of Chemical Physics*, 131, 104705.

[83] Berezhkovskii, A.M. Dagdug, L. Makhnovskii, Y.A. and Zitserman, V.Y. (2010), 'Communications: Drift and diffusion in a tube of periodically varying diameter. Driving force induced intermittency', *The Journal of Chemical Physics*, 132, 221104.

[84] Borromeo, M. and Marchesoni, F. (2010), 'Particle transport in a two-dimensional septate channel', *Chemical Physics*, 375, 2 - 3, pp. 536 - 539.

[85] Marchesoni, F. (2010), 'Mobility in periodic channels formed by cylindrical cavities', *The Journal of Chemical Physics*, 132, 166101.

[86] Hänggi. P. Marchesoni. F. Savel'ev, S. and Schmid, G. (2010), 'Asymmetry in shape causing absolute negative mobility', {Physical Review E, 82, 041121.

[87] Mondal, D. and Ray, D.S. (2010), 'Diffusion over an entropic barrier: Non-Arrenhenius behavior', *Physical Review E*, 82, 032103.

[88] Mondal, D. Das, M. and Ray, D.S. (2010), 'Entropic resonant activation', *The Journal of Chemical Physics*, 132, 224102.

[89] Savel'ev, S. Marchesoni, F. and Nori, F. (2003), 'Controlling transport in mixtures of interacting particles using Brownian motors', *Physical Review Letters*, 91, 010601.

[90] Olson, C.J. Reichhardt, C. and Nori, F. (1998), 'Nonequilibrium dynamic phase diagram fro vortex lattices', *Physical Review Letters*, 81, pp. 3757 - 3760.

[91] Noir, F. (1996), 'Intermittently flowing rivers of magnetic flux', *Science*, 271, 5254, pp. 1373 - 1374.

[92] Gammaitoni, L. Marchesoni. F. Menichella-Saetta, E. and Santucci, S. (1989), 'Stochastic resonance in bistable systems', *Physical Review Letters*, 62, pp. 349 - 352.

[93] Gammaitoni, L. Marchesoni, F. and Santucci, S. (1995), 'Stochastic resonance as a bona fide resonance', *Physical Review Letters*, 74, pp. 1052 - 1055.

[94] Hänggi, P. and Bartussek, R. (1996), 'Brownian Rectifiers: How to convert Brownian motion into directed transport', in Muller, S.C. and Parisi, J. (eds.) *Nonlinear Physics of Complex Systems: Lecture Notes in Physics*, Berlin: Springer-Verlag, pp. 294 - 308.

[95] Reimann, P. (2002), 'Brownian Motors: noisy transport far from equilibrium', *Physics Reports*, 361, pp. 57 - 265.

[96] Feynman, R.P. Leighton, R.B. and Sands, M. (1963), 'Ratchet and Pawl', in *The Feynman Lectures on Physics*, New York: Basic Books, pp. 46-1 - 46-9.

[97] Lade, S.J. (2008), *Ratchets: Directed transport without a bias force* [Poster]. Exhibited at Australian Institute of Physics 18th National Congress, Adelaide. 30 Nov - 5 Dec 2008.

[98] Jacobs, M.H. (1967), *Diffusion Processes*, New York, Springer-Verlag.

[99] Denisov, S. Flach, S. and Hänggi, P. (2014), 'Tunable transport with broken space-time symmetries', *Physics Reports*, 538, pp. 77 - 120.

[100] Cole, D. Bending, S. Savel'ev, S.E. Grigorenko, A. Tsuyoshi, T. and Nori, F. (2006), 'Ratchet without spatial asymmetry for controlling the motion of magnetic flux quanta using time-asymmetric drives,' *Nature Materials*, 5, pp. 305 - 311.

[101] Denisov, S. Flach, S. Ovchinnikov, A.A. Yevtushenko, O. and Zolotaryuk, Y. (2002), 'Broken space-time symmetries and mechanisms of rectification of ac fields by nonlinear (non)adiabatic response', *Physical Review E*, 66, 041104.

[102] Eichhorn, R. Reimann, P. and Hänggi, P. (2002), 'Brownian motion exhibiting absolute negative mobility', *Physical Review Letters*, 88, 190601.

[103] Eichhorn, R. Reimann, P. and Hänggi, P. (2002), 'Paradoxical motion of a single Brownian particle: Absolute negative mobility', *Physical Review E*, 66, 066132.

[104] Baraban, L. Makarov, D. Streubel, R. Mönch, I. Grimm, D. Sanchez, S. and Schmidt. O.G. (2012), 'Chip: deterministic motion for targeted cargo delivery', 6, 4, pp. 3383 - 3389.

[105] Ghosh, P.K. Hänggi, P. Marchesoni, F. and Nori, F. (2014), 'Giant negative mobility of Janus particles in a corrugated channel', *Physical Review E*, 89, 062115.

[106] Van Kampen, N.G. (ed.), (2007), *Stochastic processes in physics and chemistry*, 3rd edn, London: Elsevier.

[107] Higham, D.J. (2001), 'An algorithmic introduction to numerical simulation of stochastic differential equations', *Society for Industrial and Applied Mathematics*, 43, 3, pp. 525 - 546.

[108] Silhanek. A.V, Van de Vondel. J, and Moshchalkov. V.V, (2010), 'Chapter 1 Guided Vortex Motion and Vortex Ratchets in Nanostructured Superconductors', Moshchalkov, V.V. Wordenweber, R. Wolfgang, L. (eds) *Nanoscience and Engineering in Superconductivity*, Springer, pp. 1 - 24.

[109] Cole, D. Bending, S. Savel'ev, S. Grigorenko, A. Tamegai, T. Nori, F. (2006), 'Ratchet without spatial asymmetry: Controlling the motion of magnetic flux quanta using time-asymmetric drives', *Nature Materials*, 5, pp 305 - 311.

[110] Goychuk, I. and Hänggi, P. (2003), 'Non-Markovian stochastic resonance', *Physical Review Letters*, 91, 7, 070601.

[111] Goychuk, I. and Hänggi, P. (2005), 'Non-Markovian stochastic resonance: Three state model of ion channel gating', *Physical Review E*, 061906.

[112] Tinkham, M. (2004), *Superconductivity* 2nd edn, New York, Dover Books.

[113] Poole, C.P. Farach, H.A. Creswick, R.J, and Prozorov, R. (2010), *Superconductivity*, 2nd edn, London, Academic Press.

[114] Blatter, G. Feigel'man, M.V. Geshkenbein, V.B. Larkin, A.I. Vinokur, V.M. (1994), 'vortices in high temperature superconductors', *Reviews of Modern Physics* 66, 4, pp. 1125 - 1388.

[115] Eichhorn, R. Reimann, P. and Hänggi, (2002), 'Brownian motion exhibiting absolute negative mobility', *Physical Review Letters*, 88, 19, 190601.

[116] Eichhorn, R. Reimann, P. and Hänggi, (2003), 'Absolute negative mobility and current reversals of a meandering Brownian particle', *Physica A*, 325, pp. 101 - 109.

[117] Hänggi, P. Marchesoni, F. Savel'ev, S. Schmid, G. (2010), 'Asymmetry in shape causing absolute negative mobility', *Physical Review E*, 82, 041121.

[118] Web of Knowledge, (2015), Available at: http://cm.webofknowledge.com/viewCitationTree.do, (Accessed 07 March 2015).

[119] Zhu, B.Y. Marchesoni, F. and Nori, F. (2004), 'Controlling the motion of magnetic flux quanta', *Physical Review Letters*, 92, 180602.

[120] Villegas, J.E. Savel'ev, S. Nori, F. Gonzalez, E.M. Anguita, J.V. Garcia, R. and Vicent, J.L. (2003), 'A superconducting reversible rectifier that controls the motion of magnetic flux quanta', *Science*, 302, 5648, pp. 1188 - 1191.

[121] de Souza Silva, C.C. de Vondel, J.V. Morelle, M. and Moshchaikov, V.V. (2006), 'Controlled multiple reversals of a ratchet effect', *Nature* 440, pp. 651 - 654.

[122] Togawa, Y. Harada, K. Akashi, T. Kasai, H. Matsuda, T. Nori, F. Maeda, A. (2005), 'Direct observation of rectified motion of vortices in a niobium superconductor', *Physical Review Letters*, 95, 087002.

[123] Cole, D. Bending, S. Savel'ev, S. Grigorenko, A. Tamegai, T. and Nori, F. (2006), 'Ratchet without spatial asymmetry for controlling the motion of magnetic flux quanta using time-asymmetric drives', *Nature Materials*, 5, pp. 305 - 311.

[124] Nori, F. (2006), 'Nanotechnology: Reversible diodes for moving quanta', *Nature Physics*, 2, pp. 227 - 228.

[125] Marchesoni, F. (1986), 'Harmonic mixing signal: Doubly dithered ring laser gyroscope', *Physical Letters A*, 119, 5, pp. 221 - 224.

[126] Savel'ev, S. Marchesoni, F. Hänggi, P, Nori, F. (2004), 'Nonlinear signal mixing in a ratchet device', *Europhysics letters*, 67, 179, 101209.

[127] Savel'ev, S. Marchesoni, F. Hänggi, P, Nori, F. (2004), 'Transport via nonlinear signal mixing in ratchet devices', *Physical Review E*, 70, 066109.

[128] Savel'ev, S. Marchesoni, F. Hänggi, P, Nori, F. (2004), 'Signal mixing in a ratchet device: commensurability and current control', *The European Physical Journal B*, 40, pp. 403 - 408.

[129] Savel'ev, S. Marchesoni, F. and Nori, F. (2004), 'Manipulating small particles in mixtures far from equilibrium', *Physical Review Letters*, 92, 160602.

[130] Hess, H.F. Robinson, R.B. Dynes, R.C. Valles Jr, J.M. and Waszczak, J.V. (1989), 'Scanning-tunnelling-microscope observation of the Abrikosov flux lattice and the density of states near and inside a fluxoid', *Physical Review Letters*, 62, 2, pp. 214 - 216.

[131] Benzi, R. Sutera, A. and Vulpiani, A. (1981), 'The mechanism of stochastic resonance', *Journal of Physics A*, 14, pp. 453 - 457.